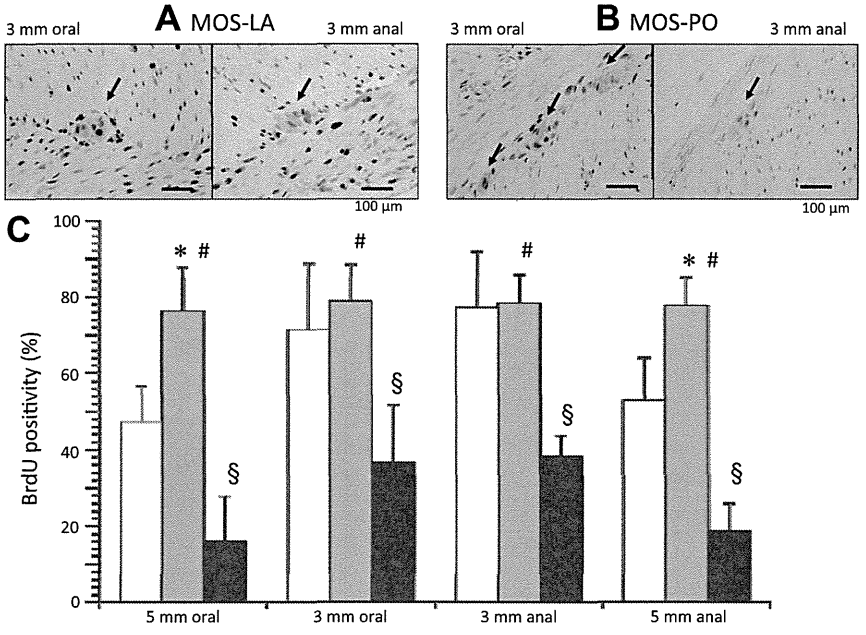

Fig. 7. Representative images of immunostaining for 5-bromo-2′-deoxyuridine (BrdU) in MOS-LA (*A*) and MOS-PO (*B*). Myenteric ganglionic cells labeled for BrdU (indicated by 6 thick arrows) were found in the rectal tissue within sites 3 mm oral and 3 mm anal from rectal anastomotic site in rats treated with 100 μmol/l MOS-LA and MOS-PO for 2 wk. Calibration bar, 100 μm. *C*: summarized data of BrdU positivity in the rectal tissue within sites 3–5 mm oral and anal from rectal anastomotic site. Open bars, MOS-LA; gray bars, MOS-PO; filled bars, SSRI-LA. $*P < 0.005$ vs. MOS-LA; $\#P < 0.005$ vs. SSRI-LA; $\S P < 0.005$ vs. MOS-LA.

erative ileus (26). Regardless of the roles of increased endogenous 5-HT in inflammation, there is a possibility for diverse actions of increased endogenous 5-HT on in vivo induction of nerve fiber tract growth across the anastomosis mediated through different subtypes of 5-HT receptors.

5-HT per se enhanced in vitro differentiation of neural networks in ES cell-induced gutlike organ in mouse (20). Moreover, it has been described that 5-HT_{2B} receptors play a role in promotion of neuronal precursor differentiation of ENS during development in mice (4). However, in the present study, SSRI did not induce in vivo nerve fiber tract growth. It is speculated that promoting effects of increased endogenous 5-HT on the nerve fiber tract growth across the anastomosis may be masked by activation of different subtypes of 5-HT receptors with suppressive effects. In addition, the increase of endogenous 5-HT may not be attainable in this region.

On the other hand, the finding that SSRI treatment induced significant decreases in number of PCNA-, DLX2-, and SR4-positive cells in the implanted GS at the neck may suggest the possibility that SSRI suppresses the mobi-

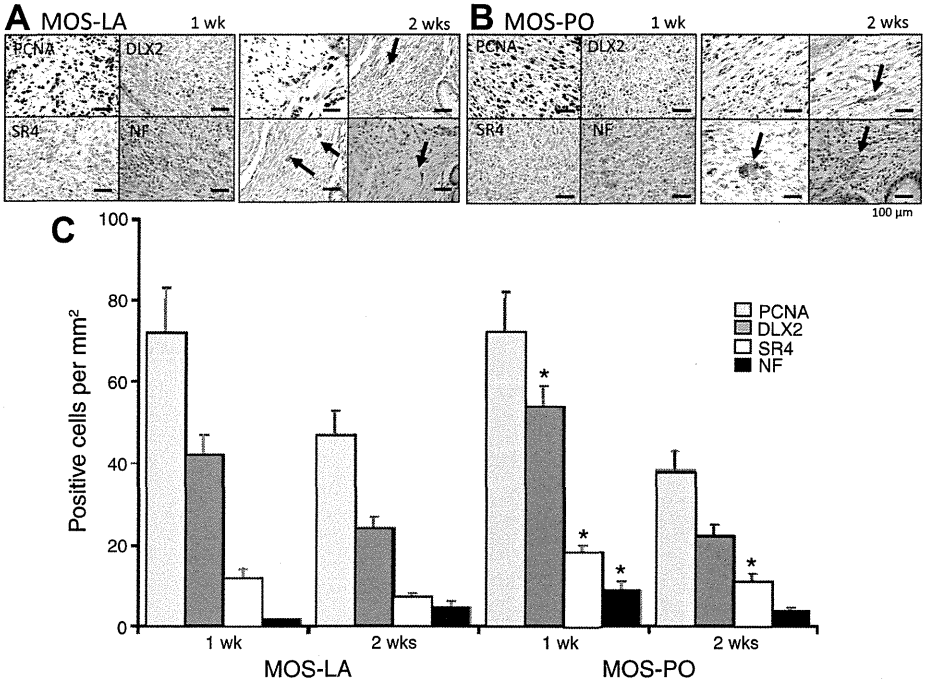

Fig. 8. Representative images of immunostaining for PCNA, DLX2, SR4, and NF in newly formed granulation tissue within the anastomotic site treated with MOS-LA (*A*) and MOS-PO (*B*) for 1 wk and 2 wk. PCNA-positive cells were detected similarly in *A* and *B*, but DLX2-, SR4- and NF-positive cells were more frequently detected at 1 wk in *B*. DLX2-, SR4-, and NF-positive cells were detected similarly at 2 wk in *A* and *B* except for SR4-positive cells. Calibration bar, 100 μm. *C*: mean values were obtained from 5 HPFs (0.2 mm^2). PCNA-positive cells were detected similarly in MOS-LA and MOS-PO, but DLX2-, SR4-, and NF- positive cells were significantly increased at 1 wk and SR4-positive cells were significantly increased at 2 wk in the granulation tissue in MOS-PO. $*P < 0.05$ vs. MOS-LA by Mann-Whitney *U*-test.

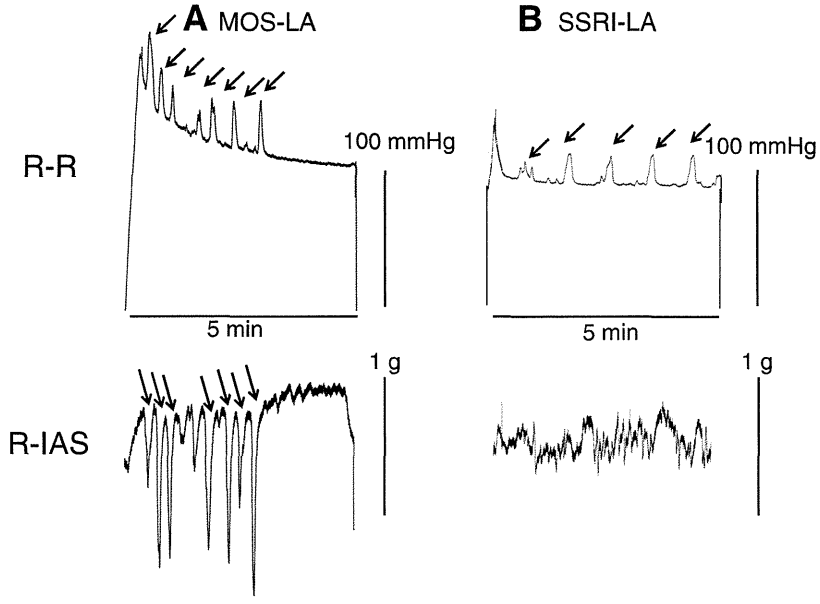

Fig. 9. Representative tracings of the recto-rectal (R-R) reflex contractile response and the recto-internal anal sphincter (R-IAS) reflex relaxation response. *A*: traces from a guinea pig treated with MOS-LA for 2 wk. Arrows indicate simultaneous R contractions and IAS relaxations. *B*: traces from a guinea pig treated with SSRI-LA for 2 wk. Arrows indicate R contractions without IAS relaxations.

lization of neural crest-derived stem cells or mesenchymal stem cells and/or differentiation into neural stem cells (see Figs. 4 and 5). In the present RT + RA model, a similar mechanism may participate in the lack of induction of nerve fiber tract growth across the anastomosis by SSRI-LA.

Furthermore, recent studies suggested that a serotonergic depressant, fluoxetine, can reverse the established state of neuronal maturation in the adult hippocampus (8) and promote gliogenesis during neural differentiation in mouse ES cells (11). Therefore, these actions of SSRI may suppress enteric neural differentiation/development as repairing mechanism even in the present adult rat.

The MOS-induced significant increase in number of DLX2-, SR4-, and c-RET-positive cells and mRNA of DLX2, SR4, and c-RET in the implanted GS at the neck could support the possibility that MOS differentiated neural crest stem-derived stem cells (17) or bone marrow mesenchymal stem cells into neural stem cells as repairing mechanisms (see Figs. 4 and 5). In the present RT + RA model, a similar mechanism may participate in induction of nerve fiber tract growth across the anastomosis by MOS-LA and by MOS-PO.

Furthermore, surprisingly, unlike in guinea pigs, MOS-LA and MOS-PO generated BrdU-positive neural cells in ganglia 3–5 mm distant from the anastomotic site 2 wk after RT + RA. The cell proliferative ability of rat neural stem cells seems to be higher than that in guinea pig.

To detect whether any drug treatments promote reconstruction of enteric neural circuit injury in the distal gut, it should be determined whether the IAS relaxation reflex (22–25, 29) can completely recover, as seen in guinea pigs (6, 15, 16). However, we did not detect a marked R-IAS relaxation reflex even in intact rats. Therefore, it was impossible to confirm the functional recovery of the IAS relaxation reflex to determine whether MOS promotes induction of nerve fiber tract growth across the anastomosis for the reflex in rats, although genetically modified rats such as SERT knockout rats (Slc6a4^{1Hubr}) (18) are available and promising for further study.

Therefore, we used guinea pigs instead of rats to evaluate the reflex index for R-IAS reflex as previously reported (15). The R-IAS reflex response remained abolished with unchanged R-R reflex in guinea pigs treated for 2 wk with SSRI-LA (Fig. 9*B*), whereas R-IAS reflex recovered to ~0.8 of intact control (= 1.0) in guinea pigs treated with MOS-LA, consistent with the previous report (15).

In conclusion, SSRI does not induce in vivo nerve fiber tract growth across the anastomosis in the rat distal gut, whereas MOS does induce nerve fiber tract growth across the anastomosis, mediated through enteric neural 5-HT$_4$ receptors.

ACKNOWLEDGMENTS

We thank Prof. Gary Mawe in the Department of Anatomy and Neurobiology of the University of Vermont for his critical reading of this manuscript.

GRANTS

This work was supported by Grants-in-Aid for Scientific Research (20659210 and 23390330 for M. Takaki, 22591491 for H. Fujii, 22591798 for H. Matsuyoshi, and 23591969 for H. Misawa) from the Ministry of Education, Science, Sports and Culture of Japan.

DISCLOSURES

No conflicts of interest, financial or otherwise, are declared by the author(s).

AUTHOR CONTRIBUTIONS

Author contributions: I.K., H.K., H. Matsuyoshi, K.G., K.O., H. Misawa, and M.T. performed experiments; I.K., H.K., and M.T. analyzed data; I.K., H.K., K.G., and M.T. prepared figures; I.K., H.K., H. Matsuyoshi, K.G., K.O., H. Misawa, H.F., and M.T. approved final version of manuscript; H.K. and M.T. interpreted results of experiments; H.F. and M.T. conception and design of research; M.T. drafted manuscript; M.T. edited and revised manuscript.

REFERENCES

1. **Bertrand PP, Barajas-Espinosa A, Neshat S, Bertrand RL, Lomax AE.** Analysis of real-time serotonin (5-HT) availability during experimental colitis in mouse. *Am J Physiol Gastrointest Liver Physiol* 298: G446–G455, 2010.
2. **Bishoff SC, Mailer R, Pabst O, Weier G, Sedlik W, Li Z, Chen JJ, Murphy DL, Gershon MD.** Role of serotonin in intestinal inflammation: knockout of serotonin reuptake transporter exacerbates 2,4,6-trinitrobenzene sulfonic acid colitis in mice. *Am J Physiol Gastrointest Liver Physiol* 296: G685–G695, 2009.
3. **Corvetti G, Fornaro M, Geuna S, Poncino A, Giacobini-Robecchi MG.** Unscheduled DNA synthesis in rat adult myenteric neurons: an immunohistochemical study. *Neuroreport* 12: 2165–2168, 2001.
4. **Fiorica-Howells E, Maroteaux L, Gershon MD.** Setotonin and the 5-HT_{2B} receptor in the development of enteric neurons. *J Neurosci* 20: 294–305, 2000.
5. **Gershon MD.** Genes and lineages in the formation of the enteric nervous system. *Curr Opin Neurobiol* 7: 101–109, 1997.
6. **Katsui R, Kojima Y, Kuniyasu H, Shimizu J, Koyama F, Fujii H, Nakajima Y, Takaki M.** A new possibility for repairing the anal dysfunction by promoting regeneration of the reflex pathways in the enteric nervous system. *Am J Physiol Gastrointest Liver Physiol* 294: G1084–G1093, 2008.
7. **Kimberly A, Moore EJO, Daniel W.** 5-HT_3 receptors mediate inflammation-induced unmasking of functional tachykinin responses in vitro. *J Appl Physiol* 92: 2529–2534, 2002.
8. **Kobayashi K, Ikeda Y, Sakai A, Yamasaki N, Haneda E, Miyakawa T, Suzuki H.** Reversal of hippocampal neuronal maturation by serotonergic antidepressants. *Proc Natl Acad Sci USA* 107: 8434–8439, 2010.
9. **Kojima Y, Nakagawa T, Katsui R, Fujii H, Nakajima Y, Takaki M.** A 5-HT_4 agonist, mosapride, enhances intrinsic rectorectal and rectoanal reflexes after removal of extrinsic nerves in guinea pigs. *Am J Physiol Gastrointest Liver Physiol* 289: G351–G360, 2005.
10. **Kojima Y, Fujii H, Katsui R, Nakajima Y, Takaki M.** Enhancement of the intrinsic defecation reflex by mosapride, a 5-HT_4 agonist, in chronically lumbosacral denervated guinea pigs. *J Smooth Muscle Res* 42: 139–147, 2006.
11. **Kusakawa S, Nakamura K, Miyamoto Y, Sanbe A, Torii T, Yamauchi J, Tanoue A.** Fluoxetine promotes gliogenesis during neural differentiation in mouse embryonic stem cells. *J Neurosci Res* 88: 3479–3487, 2010.
12. **Liu M, Gershon MD.** Neuroprotective/trophic effects of 5-HT_4 receptor stimulation on enteric neurons of mice. *Neurogastroenterol Motil* 18: 780–781, 2006.
13. **Liu MT, Kuan YH, Wang J, Hen R, Gershon MD.** 5-HT_4 receptor-mediated neuroprotection and neurogenesis in the enteric nervous system of adult mice. *J Neurosci* 29: 9683–9699, 2009.
14. **Liu Z, Sakakibara R, Odaka T, Uchiyama T, Uchiyama T, Yamamoto T, Ito T, Asahina M, Yamaguchi K, Yamaguchi T, Hattori T.** Mosapride citrate, a novel 5-HT_4 agonist and partial 5-HT_3 antagonist, ameliorates constipation in parkinsonian patients. *Mov Disord* 20: 680–686, 2005.
15. **Matsuyoshi H, Katsui R, Okumura M, Kuniyasu H, Takaki M.** 5-HT_4 receptor agonist promotes regeneration of the reflex pathways in the enteric nervous system. *J Physiol Sci* 59, *Suppl* 1: 476, 2009.
16. **Matsuyoshi H, Kuniyasu H, Okumura M, Misawa H, Katsui R, Zhang GX, Obata K, Takaki M.** A 5-HT_4-receptor activation-induced neural plasticity enhances in vivo reconstructs of enteric nerve circuit insult. *Neurogastroenterol Motil* 22: 806–813, 2010.
17. **Nagoshi N, Shibata S, Kubota Y, Nakamura M, Nagai Y, Satoh E, Matsuzaki Y, Toyama Y, Okano H.** Ontogeny and multipotency of neural crest-derived stem cells in mouse bone marrow, dorsal root ganglia, and whisker pad. *Cell Stem Cell* 2: 392–403, 2008.
18. **Olivier JD, Van Der Hart MG, Van Swelm RP, Dederen PJ, Homberg JR, Cremers T, Deen PM, Cuppen E, Cools AR, Ellenbroek BA.** A study in male and female 5-HT transporter knockout rats: an animal model for anxiety and depression disorders. *Neuroscience* 152: 573–584, 2008.
19. **Shimatani H, Kojima Y, Kadowaki M, Nakagawa T, Fujii H, Nakajima Y, Takaki M.** A 5-HT_4 agonist mosapride enhances rectorectal and rectoanal reflexes in guinea pigs. *Am J Physiol Gastrointest Liver Physiol* 285: G389–G395, 2003.
20. **Takaki M, Misawa H, Matsuyoshi H, Kawahara I, Goto K, Zhang GX, Obata K, Kuniyasu H.** In vitro enhanced differentiation of neural networks in ES gut-like organ from mouse ES cells by a 5-HT_4-receptor activation. *Biochem Biophys Res Commun* 406: 529–533, 2011.
21. **Takaki M, Nakayama S, Misawa H, Nakagawa T, Kuniyasu H.** In vitro formation of enteric neural network structure in a gut-like organ differentiated from mouse embryonic stem cells. *Stem Cells* 24: 1414–1422, 2006.
22. **Takaki M, Neya T, Nakayama S.** Sympathetic activity in the recto-rectal reflex of the guinea pig. *Pflügers Arch* 388: 45–52, 1980.
23. **Takaki M, Neya T, Nakayama S.** Role and localization of a region in the pons which has a descending inhibitory influence on sympathetically mediated inhibition of the recto-rectal reflex of guinea pigs. *Pflügers Arch* 398: 120–125, 1983.
24. **Takaki M, Neya T, Nakayama S.** Pelvic afferent reflex control of rectal motility and lumbar colonic efferent discharge mediated by the pontine sympatho-inhibitory region in guinea pigs. *Pflügers Arch* 403: 164–169, 1985.
25. **Takaki M, Neya T, Nakayama S.** Functional role of lumbar sympathetic nerves and supraspinal mechanism in the defecation reflex of the cat. *Acta Med Okayama* 41: 249–257, 1987.
26. **Tsuchida Y, Hatao F, Fujisawa M, Murata T, Kaminishi M, Seto Y, Hori M, Ozaki H.** Neuronal stimulation with 5-hydroxytryptamine 4 receptor induces anti-inflammatory actions via α7nACh receptors on muscularis macrophages associated with postoperative ileus. *Gut* 60: 631–637, 2011.
27. **Willaime-Morawek S, Seaberg RM, Batista C, Labbe E, Attisano L, Gorski JA, Jones KR, Kam A, Morshead CM, van der Kooy D.** Embryonic cortical neural stem cells migrate ventrally and persist as postnatal striatal stem cells. *J Cell Biol* 175: 159–168, 2006.
28. **Wood JD.** Enteric nervous system neuropathy: repair and restoration. *Curr Opin Gastroenterol* 27: 106–111, 2011.
29. **Yamanouchi M, Shimatani H, Kadowaki M, Yoneda S, Nakagawa T, Fujii H, Takaki M.** Integrative control of rectoanal reflex in guinea pigs through lumbar colonic nerves. *Am J Physiol Gastrointest Liver Physiol* 283: G148–G156, 2002.

Cancer Science
The official journal of the Japanese Cancer Association JCA

Significance of epithelial growth factor in the epithelial–mesenchymal transition of human gallbladder cancer cells

Takamitsu Sasaki,[1] Hiroki Kuniyasu,[2,3] Yi Luo,[2] Daisuke Kato,[1] Satoshi Shinya,[1] Kiyomu Fujii,[2] Hitoshi Ohmori[2] and Yuichi Yamashita[1]

[1]Department of Gastroenterolgical Surgery, Fukuoka University School of Medicine, Fukuoka; [2]Department of Molecular Pathology, Nara Medical University, Kashihara, Japan

(Received November 17, 2011/Revised February 28, 2012/Accepted March 3, 2012/Accepted manuscript online March 8, 2012)

Five gallbladder cancer (GBC) cell lines were examined for morphological changes in collagen gel culture. GBh3 and HUCCT-1 cells formed tubules in response to treatment with epithelial growth factor (EGF) and hepatocyte growth factor (HGF), and showed high levels of expression of E-cadherin (ECD), and low levels of SNAIL, vimentin, transforming growth factor (TGF)-β, and nucleostemin (NS). In contrast, the GBd15 and FU-GBC-1 cell lines treated with EGF and HGF showed a scattering phenotype, and expressed low levels of ECD and high levels of SNAIL, vimentin, TGF-β, and NS. All cell lines expressed the EGF receptor, c-Met, EGF, and TGF-α, but not HGF. Transforming growth factor-β was upregulated by EGF. Knockdown of the EGF receptor abrogated both tubule formation and scattering, whereas KD of TGF-β abrogated only scattering. Knockdown of EGF induced nuclear translocation of β-catenin and Wnt-related NS induction in the scattering cell lines, but not in the tubule-forming cell lines, whereas KD of glycogen synthase kinase-3β in the tubule-forming cell lines resulted in the nuclear translocation of β-catenin and Wnt-related NS induction in response to EGF treatment. These results suggest that EGF enhances epithelial–mesenchymal transformation and acquisition of stemness in GBC cells with a scattering phenotype through the activity of β-catenin. Repression of ECD in scattering GBC cells induced the release of β-catenin from the cell adhesion complexes along the plasma membrane and its translocation to the nucleus to activate Wnt signaling, which upregulated NS. (*Cancer Sci*, doi: 10.1111/j.1349-7006.2012.02264.x, 2012)

Biliary tract cancer is the sixth leading cause (5.1%) of cancer death in Japan, with 17 000 BTC patients dying in 2009.[1] Biliary tract cancer shows poor prognosis in spite of aggressive treatment, and the 5-year survival is only 18%.[1] Nodal metastasis is the most significant prognostic factor for GBC.[2–4]

Epithelial growth factor receptor is a key factor in epithelial malignancies, and its activity enhances tumor growth, invasion, and metastasis.[5] Biliary tract cancers express EGFR in 60.7% of cases.[6] The EGFR-overexpressing GBC cases show poorly differentiated histology and decreased survival of 1.5 years in median survival.[7] Amplification and point mutations of the EGFR gene have been reported to be 1% and 15–26.5%, respectively, in GBC.[8–10] The HGF receptor c-Met is involved in the early carcinogenesis of BTC.[11] c-Met is expressed in 74% of invasive GBC and is associated with invasive depth.[12] Because HGF is secreted from fibroblasts, c-Met activation depends on the cancer–host interaction.[13] Transforming growth factor-β is widely expressed in advanced GBC and is associated with angiogenesis and tumor-associated macrophage infiltration as well as with stromal fibrosis.[14,15]

Epidermal growth factor receptor, c-Met, and TGF-β have recently been implicated in the process of EMT.[16–19] Epithelial–mesenchymal transition comprises a switch in cell differentiation from polarized epithelial cells to contractile and motile mesenchymal cells.[20] In EMT-type cells, the reduction of the epithelial marker ECD occurs in parallel with the induction of the mesenchymal marker VIM.[21] Epithelial–mesenchymal transition occurs during cancer progression and enhances invasion and metastasis.[20]

The present study aimed to clarify the relationship between morphogenesis, EMT, and growth factors in GBC cells.

Materials and Methods

Cell culture and reagents. Human GBC cell lines GBh3, HUCCT-1, FU-GBC-1, FU-GBC-2, and GBd15 were maintained in DMEM (Sigma, St. Louis, MO, USA) containing 10% FBS (Sigma) under the conditions of 5% CO_2 in air at 37°C. Human recombinant EGF (Peprotec EC, Rocky Hill, NJ, USA), human recombinant HGF (R&D Systems, Minneapolis, MN, USA), and Wnt inhibitor (IWP3; Miltenyi Biotec, Bergisch Gladbach, Germany) were purchased. The effect of various concentrations of EGF (1, 5, 10, 25, 50, 100 ng/mL) and HGF (1, 10, 30, 60, 120 ng/mL) on morphology was examined in GBC cells. At 10 ng/mL and higher concentrations of EGF, and at 30 ng/mL and higher concentrations of HGF, there were clear effects on cell morphology (see Fig. 1).

Collagen gel assay. Before preparing the gels, 1 mL of 0.1% BSA (Sigma) solution was added into each well of a 48-well plate and incubated at 37°C for 1 h. A collagen solution mixture was prepared by quickly mixing eight volumes of collagen type I solution (Nitta Gelatin, Tokyo, Japan) with one volume of 10-fold concentrated DMEM and one volume of sodium bicarbonate (22 mg/mL). Cells (1×10^6) were added to 300 μL collagen solution mixture, and gently mixed. Collagen solution was poured into a 48-well plate after BSA solution was removed, and allowed to gel for 30 min in a 5% CO_2 atmosphere at 37°C. After 30 min, culture media was poured into each well, and the collagen gels were detached from the surface of the well by rimming the gels with a sterile needle and gently swirling the plate.

Short interfering RNA. FlexiTube siRNAs for EGFR, c-Met, TGF-β, and GSK-3β were purchased from Qiagen Genomics (Bothell, WA, USA). AllStars Negative Control siRNA was used for control (Qiagen Genomics). Cells were transfected with 50 nM siRNA for each gene using Lipofectamine 2000

[3]To whom correspondence should be addressed.
E-mail: cooninh@zb4.so-net.ne.jp

doi: 10.1111/j.1349-7006.2012.02264.x

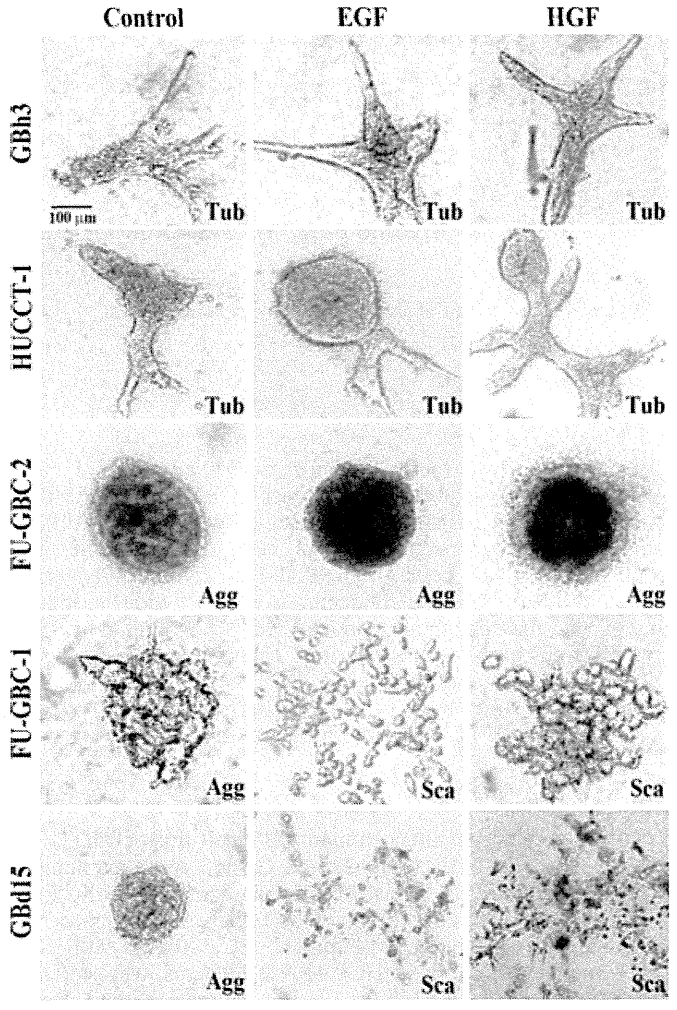

Fig. 1. Effect of epidermal growth factor (EGF) and hepatocyte growth factor (HGF) on the morphogenesis of gallbladder cancer cells grown on collagen gels. Five gallbladder cell lines were treated with EGF (10 ng/mL) or HGF (30 ng/mL) in collagen gel for 48 h. The cells showed tubule formation (Tub), cell aggregation (Agg), or scattering (Sca). Bar, 100 μm.

(Invitrogen, Carlsbad, CA, USA) according to the manufacturer's instructions.

Quantitative RT-PCR. Total RNA (1 μg) was synthesized with the ReverTra Ace qPCR RT Kit (Toyobo, Osaka, Japan). Quantitative RT-PCR was carried out on StepOne Real-Time PCR Systems (Applied Biosystems, Foster City, CA, USA) using Fast SYBR Green Master Mix (Applied Biosystems) and analyzed using the relative standard curve quantification method. The PCR conditions were according to the provider's instructions and the actin β mRNA level was amplified for internal control. Each amplification was evaluated by melting curve analysis and PCR products were electrophoresed on 2% agarose gel. All PCRs were carried out in triplicate at least. Primer sets were purchased from Santa Cruz Biotechnology (Santa Cruz, CA, USA). The reaction conditions were according to the provider's instructions.

Immunoblot analysis. Each fraction was extracted as described previously.[22] Twenty-five microgram lysates were subjected to immunoblot analysis in 12.5% SDS-polyacrylamide gels followed by electrotransfer to nitrocellulose filters. The filters were incubated with primary antibodies, then with peroxidase-conjugated IgG antibody (Medical and Biological Laboratories, Nagoya, Japan). Antibodies to β-catenin (Life-Span Biosciences, Seattle, WA, USA), ECD (Transduction Laboratories, Lexington, KY, USA), Twist (Abnova, Taipei City, Taiwan), ZEB-1 (Bioss, Woburn, MA, USA), and Slug (Abgent, San Diego, CA, USA) were used as primary antibodies. The immune complex was visualized with the Enhanced Chemiluminescence Western blot detection system (Amersham Biosciences, Aylesbury, UK).

Cell growth and apoptosis. Cells were seeded at a density of 10 000 cells per well in 12-well tissue culture plates. Then MTT (Sigma) was added to the culture medium at a concentration of 25 μg/mL at 1 h before harvest. The harvested cell pellets were lysed with 1 mL DMSO, and 200 μL of the lysate was examined at 620 nm. Cells were seeded at a density of 20 000 cells per wells in 96-well tissue culture plates. After cells were exposed to MTT for 1 h before the harvest, chromogenic granules from the cells were dissolved in DMSO and subjected to examination at 540 nm. The experiments were carried out three times. Apoptosis was assessed by staining with Hoechst33258 fluorescent dye (Wako Pure Chemical Industries, Osaka, Japan). The number of apoptotic cells was counted by observation of 1000 cells.

Enzyme-linked immunosorbant assay. The conditioned medium filtered through a 0.2 μm filter (Becton-Dickinson Labware, Bedford, MA, USA) was used for ELISA. Concentrations of EGF, TGF-α, and HGF were detected by their specific ELISA kits; human EGF ELISA kit and human HGF ELISA kit (Boster Biological Technology, Wuhan, China) and TGF-α DuoSet ELISA (R&D Systems) were used according to the provider's instructions.

Statistical analysis. Statistical analyses of experimental data were done by the Mann–Whitney *U*-test and ANOVA. Statistical significance was defined as a two-sided *P*-value of <0.05.

Results

Effect of EGF and HGF on morphogenesis of GBC cells. The effect of EGF and HGF on the morphogenesis of human GBC cells was first examined. The five GBC cell lines analyzed were cultured in collagen gel and treated with EGF or HGF (Fig. 1). Treatment with EGF and HGF caused tubule formation in GBh3 and HUCCT-1 cells, whereas FU-GBC-2 cells did not form tubules, but rather formed cell aggregates in response to treatment. Cell scattering was observed in GBd15 and FU-GBC-1 cells treated with EGF and HGF. Scattered cells lost polygonal epithelioid features but developed spindle fibroblastic features.

Expression of growth factors and receptors in GBC cells. The expression of growth factor receptors and production of their ligands were examined in five GBC cell lines (Fig. 2). Both EGFR and c-Met were expressed in all five cell lines at levels that were not clearly associated with morphogenetic changes. The five GBC cell lines secreted TGF-α and EGF, but not HGF, into the culture medium. The levels of EGF or TGF-α were not associated with the morphogenetic changes observed. Epidermal growth factor receptor and the ligands analyzed are considered to form an autocrine loop in the five GBC cell lines, whereas c-Met does not possess autocrine activation. Autocrine activation of EGFR is considered the cause of partial scattering of GBd15 cells.

Expression of cell adhesion-related molecules in GBC cells. Cell-to-cell adhesion molecules play a pivotal role in the morphogenesis of cancer cells.[23] The expression of ECD and β-catenin was, therefore, examined in the five GBC cell lines (Fig. 3a,b). β-Catenin expression was constitutively positive in GBC cells, whereas ECD expression levels varied in the different cell lines. Tubule-forming GBh3 and HUCCT-1 cells expressed high levels of ECD and low levels of VIM (Fig. 3c). In contrast, scattering GBd15 and FU-GBC-1 cells showed

doi: 10.1111/j.1349-7006.2012.02264.x

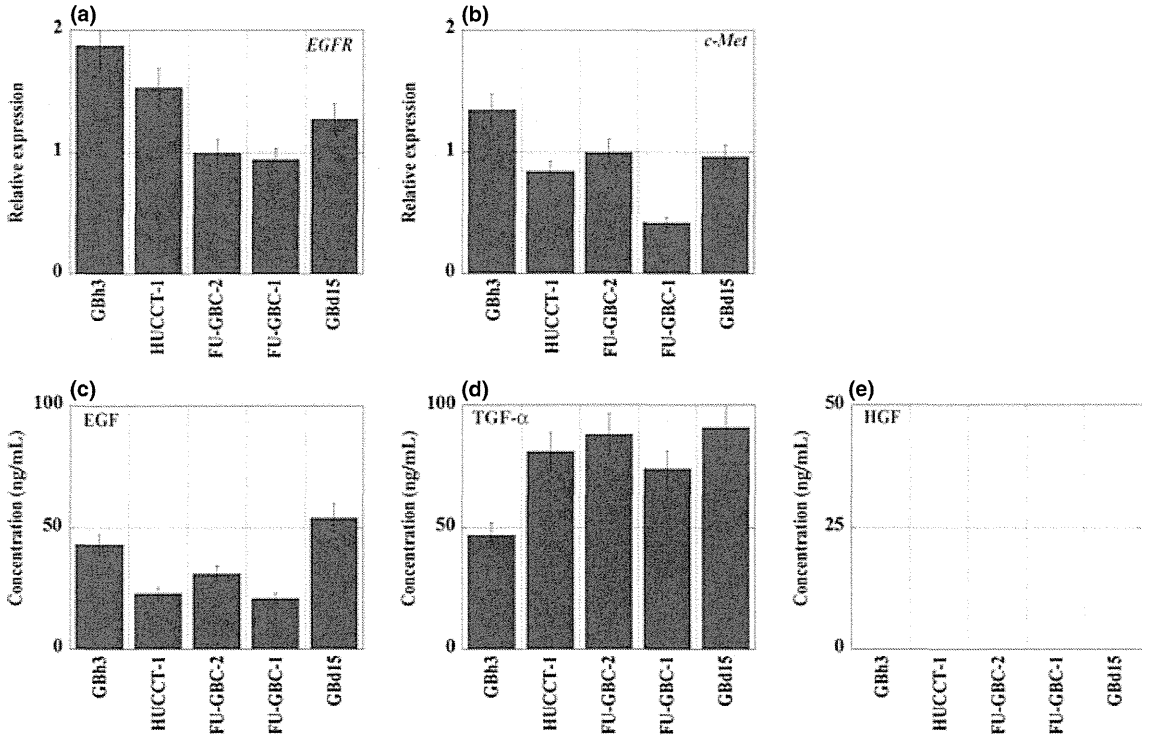

Fig. 2. Expression of growth factor receptors and ligands in gallbladder cancer cells. (a,b) The mRNA expression of epidermal growth factor receptor (EGFR) and c-Met was examined by quantitative RT-PCR. β-Actin expression was used as a standard. (c–e) Protein concentrations of epidermal growth factor (EGF), transforming growth factor (TGF)-α, and hepatocyte growth factor (HGF) were measured by ELISA. Bar, SD from three independent examinations.

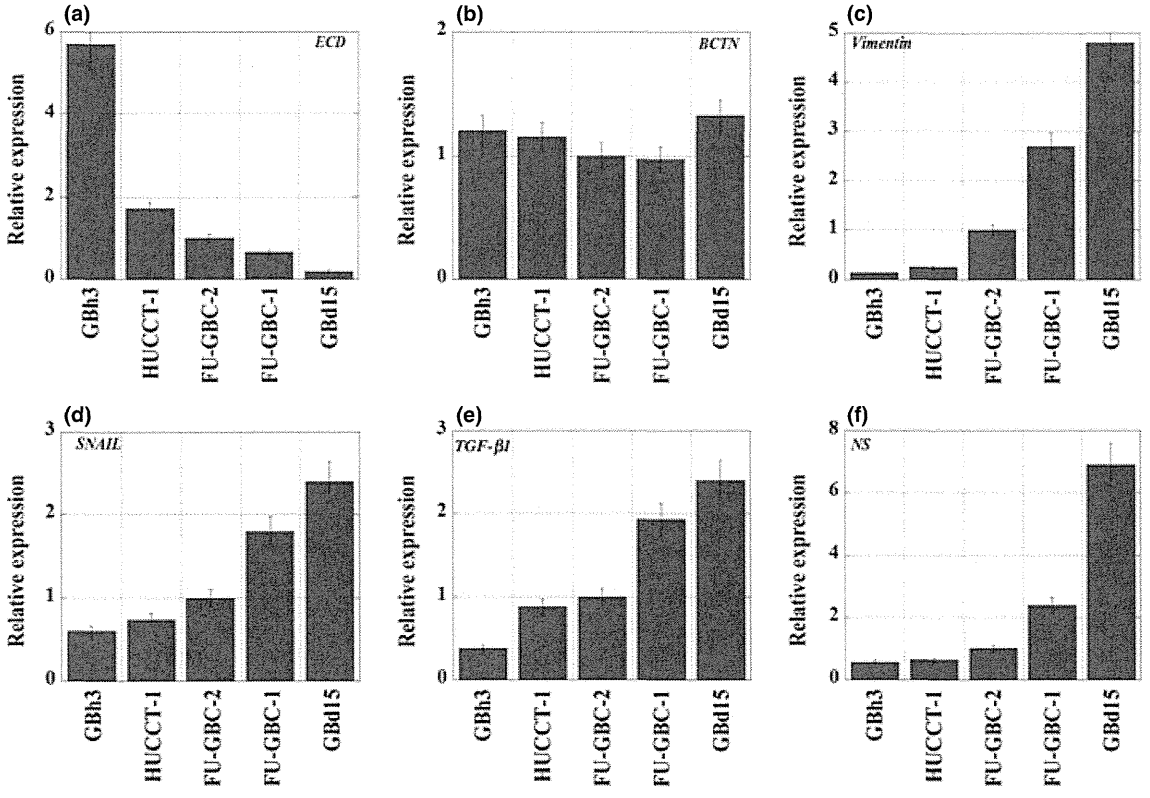

Fig. 3. Expression of epithelial–mesenchymal transition-associated genes in gallbladder cancer cells. The mRNA expressions of E-cadherin (ECD) (a), β-catenin (BCTN) (b), vimentin (c), SNAIL (d), transforming growth factor (TGF)-β1 (e), and nucleostemin (NS) (f) are shown. Expression values were normalized by β-actin expression. Bar, SD from three independent examinations.

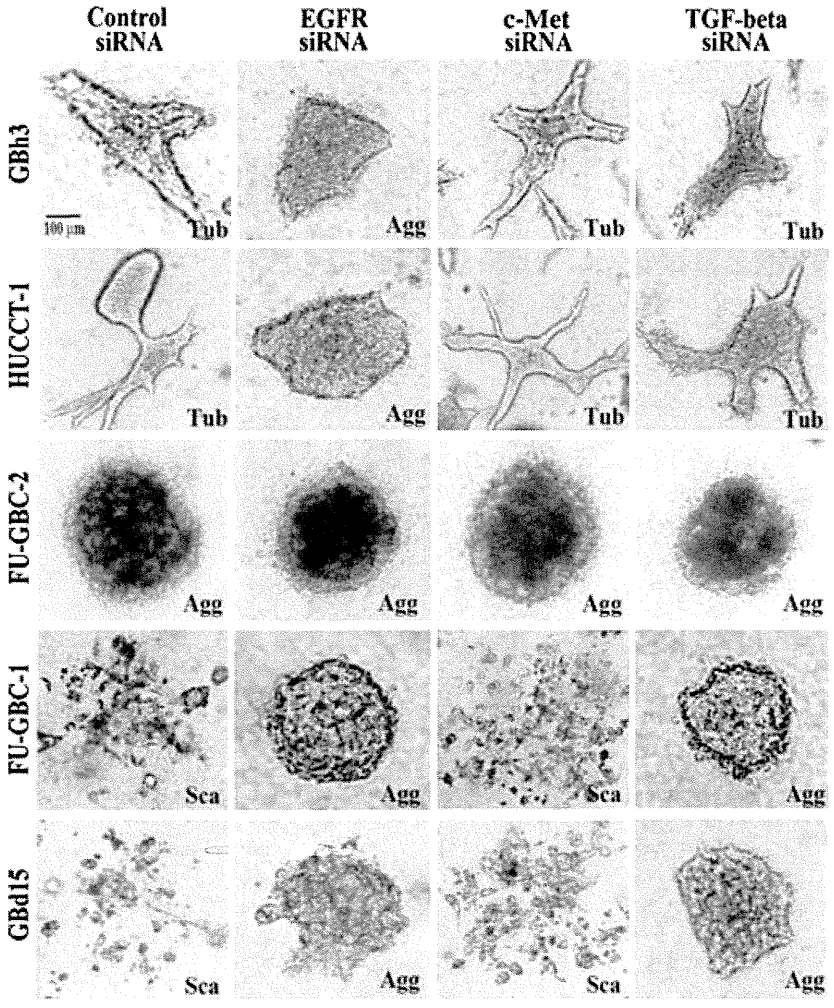

Fig. 4. Effect of knockdown of epidermal growth factor receptor (EGFR), c-Met, and transforming growth factor (TGF)-β on morphogenesis in GBC cells grown in collagen gels. Five gallbladder cell lines were transfected with siRNAs for EGFR, c-Met, and TGF-β, treated with epidermal growth factor (EGF; 10 ng/mL) and hepatocyte growth factor (HGF; 30 ng/mL) and grown in collagen gel for 48 h. The cells showed tubule formation (Tub), cell aggregation (Agg), or scattering (Sca). Bar, 100 μm.

markedly reduced ECD and upregulated VIM. Aggregate-forming FU-GBC-2 cells showed intermediate levels of ECD and VIM expression. These results suggest that the levels of ECD and VIM are closely associated with the morphogenesis of GBC cells.

Expression of EMT-associated molecules in GBC cells. Because the scattering phenotype of GBC cells resembles that of cancer cells undergoing EMT, the expression of EMT-associated molecules in the five GBC cell lines was examined (Fig. 3d–f). Scattering GBd15 and FU-GBC-1 cells showed increased expression of SNAIL, TGF-β, and NS. In contrast, tubule-forming GBh3 and HUCCT-1 cells showed low levels of SNAIL, TGF-β, and NS expression. The scattering phenotype is, therefore, thought to be linked to EMT.

Effect of KD of EGFR or TGF-β on morphogenesis of GBC cells. Because the phenotype of the five GBC cell lines involved an active EGFR autocrine loop, we examined the effect of EGFR KD on morphogenesis in the GBC cells cotreated with EGF and HGF (Fig. 4). The EGFR KD caused cell aggregation, but not tubule formation or scattering in all cell lines, suggesting that EGFR is responsible for both tubule formation and scattering.

In contrast, c-Met KD did not alter the effect of co-treatment with EGF and HGF on morphogenesis. The TGF-β KD resulted in cell aggregation in GBd15 and FU-GBC-1 cells with abrogation of scattering. However, GBh3, HUCCT-1, and FU-GBC-2 cells did not show altered morphogenesis in response to TGF-β KD. Thus, EGFR might be needed for both tubule formation and scattering, whereas c-Met might play a comparatively minor role. The activity of TGF-β might be coordinated with that of EGFR in producing the scattering phenotype.

Effect of EGF on expression of EMT-associated genes. The effect of the EGF/EGFR system on the expression of EMT-associated genes was examined in the GBh3 and GBd15 cells (Fig. 5a–d). In tubule-forming GBh3 cells, KD of EGFR and EGF treatment did not significantly alter the expression of EMT-associated genes including *SNAIL*, *Twist*, *ZEB-1*, and *Slug*. In scattering GBd15 cells, EGF treatment downregulated ECD. In contrast, EGF treatment upregulated SNAIL, Twist, ZEB-1, Slug, TGF-β, and NS expression. Inversely, EGFR KD increased ECD and decreased SNAIL, Twist, ZEB-1, Slug, TGF-β, and NS expression.

As shown in Figure 5(e,f), β-catenin localized to the cytoplasmic membrane and cytoplasm in untreated GBd15 cells, whereas in the EGF-treated cells, β-catenin was detected in the cytoplasm and nuclei. Because nuclear translocation of β-catenin reflects the activation of Wnt signaling, GBd15 cells were cotreated with EGF and a Wnt inhibitor. Although the Wnt inhibitor did not affect TGF-β expression, it downregulated NS expression. These results indicate that EGF signaling increases NS expression through β-catenin-induced Wnt activation.

doi: 10.1111/j.1349-7006.2012.02264.x

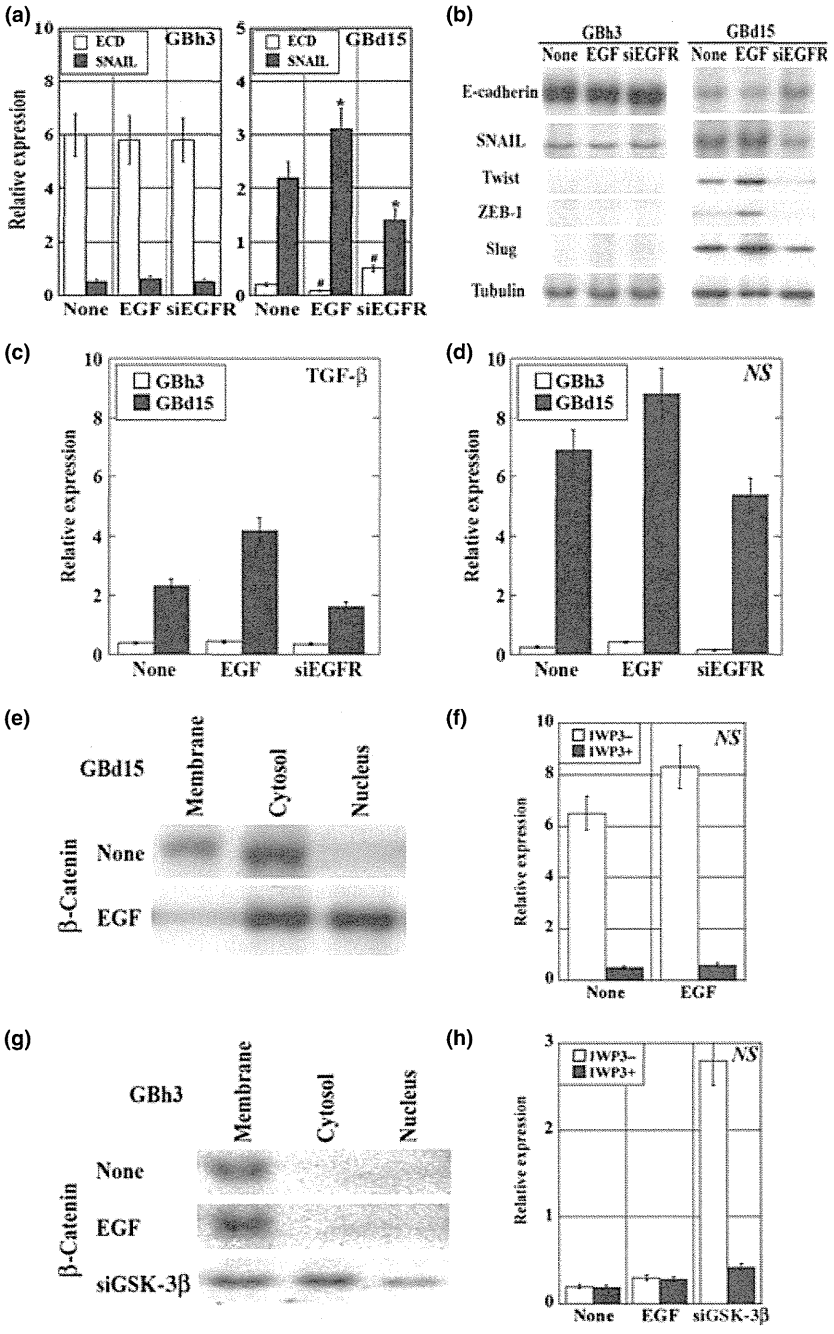

Fig. 5. Effect of epidermal growth factor (EGF) treatment and epidermal growth factor receptor (EGFR) knockdown on the expression of epithelial–mesenchymal transition-associated genes in gallbladder cancer cells. (a–d) Tubule-forming GBh3 cells and scattering GBd15 cells with or without EGFR knockdown were treated with EGF. (a) The mRNA expressions of E-cadherin (ECD) and SNAIL were examined, standardized by β-actin expression. $*P < 0.01$, $\#P < 0.001$. (b) The protein levels of ECD and SNAIL were examined by immunoblotting. The protein levels of Twist, ZEB-1, and Slug were also examined. Tubulin was examined as a loading control. (c,d) The mRNA expressions of transforming growth factor (TGF)-β and nucleostemin (NS) were examined. The expression was standardized by β-actin. (e,g) β-Catenin intracellular localization was examined in cells after EGF or glycogen synthase kinase (GSK)-3β knockdown. (f,h) Effect of the Wnt inhibitor IWP3 on NS mRNA expression in cells after EGF or GSK-3β knockdown. Bar, SD from three independent examinations.

Finally, the role of β-catenin in the EGF pathway was examined in tubule-forming GBh3 cells (Fig. 5g,h). β-Catenin localized to the cytoplasmic membrane in untreated and EGF-treated GBh3 cells. The GSK-3β KD in GBh3 cells caused the dissociation of β-catenin from the membrane-bound cell adhesion complex, which resulted in loss of tubule formation and gain of scattering. The GSK-3β KD in GBh3 cells also caused the translocation of β-catenin to the cytoplasm and nuclei. These data suggest that the location of β-catenin might determine the differential responses to EGF and the morphology of GBC cells.

Discussion

In the present study, we examined the effect of growth factors on morphogenesis and scattering of GBC cells. The scattering

phenotype of GBd15 and FU-GBC-1 cells was enhanced by treatment with EGF and HGF. Scattering cancer cells show spindle fibroblastic shape and poor cell-to-cell attachment. In the present study, these cell lines showed decreased ECD and SNAIL expression, which is a key phenotype of EMT. They also expressed TGF-β at high levels; TGF-β is closely associated with EMT induction.[19] Moreover, the scattering cell lines expressed NS at high levels. Nucleostemin is one of the stemness markers, and high NS expression is considered to be related to the acquisition of the stem cell phenotype. This pattern of expression is compatible with EMT of cancer cells.

β-Catenin is an ECD-bound cytoplasmic molecule with a link to the cytoskeleton. The dissociation of β-catenin from ECD results in its translocation into the nucleus to act as a transcription factor in Wnt activation. Mutations in the *APC* gene cause inactivation of the ECD complex and nuclear translocation of β-catenin, which is important for carcinogenesis. Thus, alterations in the ECD and β-catenin complex affect multiple pathways to enhance the malignant activity of cancer cells.

The present data showed that the EGF-induced β-catenin translocation into the nucleus occurs in the GBC cells with a scattering phenotype, and is associated with Wnt-related increase in NS. In contrast, in GBC cells with a tubule-forming phenotype, nuclear localization of β-catenin was not detected in the presence or absence of EGF. However, KD of GSK-3β resulted in nuclear translocation of β-catenin and Wnt-related NS induction. Downregulation of ECD, therefore, induces nuclear translocation of β-catenin, which subsequently increases stemness by Wnt activation. β-Catenin, therefore, plays an important role in the acquisition of stemness in the scattering GBC cells, in which ECD is repressed, inducing the release of β-catenin from the cell adhesion complex on the cytoplasmic membrane. The free β-catenin translocates to the nucleus to activate Wnt signaling, which upregulates NS. In tubule-forming GBC cells, the forced release of β-catenin from the cell adhesion complex by GSK KD caused a scattering phenotype and NS upregulation. In clinical studies, nuclear and/or cytoplasmic translocation of β-catenin was found in half of the GBC cases and was associated with poorly differentiated histology.[24]

Activation of Wnt signaling by β-catenin nuclear translocation affects the behavior of mesenchymal stem cells and also mediates EMT.[25] Moreover, EMT is linked to the acquisition of the stem cell phenotype of cancer cells.[26] Our current data is compatible with this mechanism. Gallbladder cancer cells with a scattering phenotype are thought to possess an EMT phenotype with high cancer stem cell competence, which is related to more aggressive progression and metastasis of the disease. Moreover, EMT-type cells with stemness are responsible for drug resistance.[27,28]

In our study, the EMT phenotype was closely associated with ECD expression. Gallbladder cancer cells with low ECD expression showed a scattering phenotype in response to EGFR activation, whereas GBC cells with high ECD expression showed a tubule-forming phenotype. Reduced ECD expression is found in more than 60% of GBC cases.[29,30] Downregulation of ECD is more pronounced in advanced GBC cases than in early cases, and is associated with poorer prognosis.[29] Repression of ECD is caused by promoter DNA methylation, gene mutation, and transcriptional regulation. Gene silencing of ECD by methylation of the promoter is detected in 41% of BTC cases.[31] High frequency of loss of heterozygosity of ECD is found in GBC.[30] In the negative regulation of ECD, certain transcription factors have been identified as playing a role, including ZEB-1, ZEB-2, Twist, Slug, and SNAIL.[18] These factors are observed during the EMT of cancer cells. In the present study, SNAIL expression was inversely correlated with ECD expression. Expressions of Twist, ZEB-1, and Slug were also increased by EGF treatment in association with ECD repression in GBd15 cells. In contrast, HUCCT-1 cells showed the same level of SNAIL expression as GBh3 cells, whereas ECD expression in HUCCT-1 cells was lower than that in GBh3 cells. Methylation of the promoter of the *ECD* gene was detected in HUCCT-1 cells (data not shown). Recent studies identified specific microRNAs associated with ECD repression or EMT. A candidate oncogenic miRNA, miR-21, was found to induce TGF-β-related EMT,[32] and miR-200 is downregulated in cancer cells, which results in ZEB-1/-2-related EMT.[33] These factors should be examined in GBC.

Our data showed the significance of EGFR in the induction of EMT in GBC cells. Activation of EGFR inactivates GSK-3β and upregulates SNAIL, which results in ECD repression and EMT in uterine cervical cancer.[21] Epidermal growth factor receptor also enhances ubiquitination and degradation of ECD by CDC42 activation through the Src pathway.[34] In contrast, in cells expressing ECD and showing stable cell-to-cell attachment, the activity of the EGFR–ERK pathway is decreased and β-catenin–T lymphocyte-specific transcription factor (TCF) signaling is inhibited.[35] In dense culture of ECD expressing airway epithelial cells, EGFR activation promotes cell differentiation with mucin production.[36] E-cadherin regulates EGFR by promoting the formation of a complex with the extracellular domain of ECD.[37] The intrinsic tyrosine kinase activity and dimerization of the EGFR in cells grown in sparse culture are induced by EGF, whereas these activities are not induced in cells grown in dense culture.[38] Thus, interaction between EGFR and ECD generates both tubulogenesis and scattering. Decreased ECD levels enhance EGFR-related ECD downregulation in a vicious cycle, which results in the inactivation of GSK-3β, β-catenin–Wnt activation, increment of stemness, and EMT.

In cholangiocellular carcinoma cell lines, the anti-EGFR antibody cetuximab is partially effective in EGFR-expressing cells.[39] KRAS mutations affect the efficacy of cetuximab in these cells. Gefinitib, a selective EGFR tyrosine kinase inhibitor, inhibits the phosphorylation of EGFR, ERK, and AKT, and induces G_1 arrest and apoptosis by upregulating p21 and p27, and BAX activation in GBC cells.[40] Epidermal growth factor receptor targeting is, therefore, critical in the treatment of GBC.

Acknowledgments

This work was supported in part by a Grant-in-Aid for Scientific Research from the Japan Society for the Promotion of Science, Japan, and a Grant-in-Aid for Scientific Research from the Ministry of Health, Labour and Welfare, Japan.

Disclosure Statement

The authors have no conflicts of interest.

Abbreviations

BTC	biliary tract cancer
ECD	E-cadherin
EGF	epithelial growth factor
EGFR	epithelial growth factor receptor
EMT	epithelial–mesenchymal transition
GBC	gallbladder cancer
GSK	glycogen synthase kinase
HGF	hepatocyte growth factor
KD	knockdown
NS	nucleostemin
TGF	transforming growth factor
VIM	vimentin

doi: 10.1111/j.1349-7006.2012.02264.x

References

1 Center for Cancer Control and Information Services, ed. *Current Cancer Statistics in Japan*. Tokyo, Japan: National Cancer Center, 2011. Available from URL: http://ganjoho.ncc.go.jp/public/statistics/pub/statistics01.html
2 Bartlett DL, Fong Y, Fortner JG, Brennan MF, Blumgart LH. Long-term results after resection for gallbladder cancer. Implications for staging and management. *Ann Surg* 1996; **224**: 639–46.
3 Dawes LG. Gallbladder cancer. *Cancer Treat Res* 2001; **109**: 145–55.
4 Bartlett DL. Gallbladder cancer. *Semin Surg Oncol* 2000; **19**: 145–55.
5 Normanno N, De Luca A, Bianco C *et al.* Epidermal growth factor receptor (EGFR) signaling in cancer. *Gene* 2006; **366**: 2–16.
6 Harder J, Waiz O, Otto F *et al.* EGFR and HER2 expression in advanced biliary tract cancer. *World J Gastroenterol* 2009; **15**: 4511–7.
7 Kaufman M, Mehrotra B, Limaye S *et al.* EGFR expression in gallbladder carcinoma in North America. *Int J Med Sci* 2008; **5**: 285–91.
8 Leone F, Cavalloni G, Pignochino Y *et al.* Somatic mutations of epidermal growth factor receptor in bile duct and gallbladder carcinoma. *Clin Cancer Res* 2006; **12**: 1680–5.
9 Ooi A, Suzuki S, Nakazawa K *et al.* Gene amplification of Myc and its coamplification with ERBB2 and EGFR in gallbladder adenocarcinoma. *Anticancer Res* 2009; **29**: 19–26.
10 Pignochino Y, Sarotto I, Peraldo-Neia C *et al.* Targeting EGFR/HER2 pathways enhances the antiproliferative effect of gemcitabine in biliary tract and gallbladder carcinomas. *BMC Cancer* 2010; **10**: 631.
11 Sanada Y, Osada S, Tokuyama Y *et al.* Critical role of c-Met and Ki67 in progress of biliary carcinoma. *Am Surg* 2010; **76**: 372–9.
12 Moon WS, Park HS, Lee H *et al.* Co-expression of cox-2, C-met and beta-catenin in cells forming invasive front of gallbladder cancer. *Cancer Res Treat* 2005; **37**: 171–6.
13 Matsumoto K, Date K, Shimura H, Nakamura T. Acquisition of invasive phenotype in gallbladder cancer cells via mutual interaction of stromal fibroblasts and cancer cells as mediated by hepatocyte growth factor. *Jpn J Cancer Res* 1996; **87**: 702–10.
14 Kitamura K, Kasuya K, Tsuchida A *et al.* Immunohistochemical analysis of transforming growth factor beta in gallbladder cancer. *Oncol Rep* 2003; **10**: 327–32.
15 Yukawa M, Fujimori T, Hirayama D *et al.* Expression of oncogene products and growth factors in early gallbladder cancer, advanced gallbladder cancer, and chronic cholecystitis. *Hum Pathol* 1993; **24**: 37–40.
16 Chang HY, Kao MC, Way TD, Ho CT, Fu E. Diosgenin suppresses HGF-induced epithelial-mesenchymal transition by down-regulation of MDM2 and vimentin. *J Agric Food Chem* 2011; **59**: 5357–63.
17 Barr S, Thomson S, Buck E *et al.* Bypassing cellular EGF receptor dependence through epithelial-to-mesenchymal-like transitions. *Clin Exp Metastasis* 2008; **25**: 685–93.
18 McConkey DJ, Choi W, Marquis L *et al.* Role of epithelial-to-mesenchymal transition (EMT) in drug sensitivity and metastasis in bladder cancer. *Cancer Metastasis Rev* 2009; **28**: 335–44.
19 Miyazono K. Transforming growth factor-beta signaling in epithelial-mesenchymal transition and progression of cancer. *Proc Jpn Acad Ser B Phys Biol Sci* 2009; **85**: 314–23.
20 Moustakas A, Heldin CH. Signaling networks guiding epithelial-mesenchymal transitions during embryogenesis and cancer progression. *Cancer Sci* 2007; **98**: 1512–20.
21 Lee MY, Chou CY, Tang MJ, Shen MR. Epithelial-mesenchymal transition in cervical cancer: correlation with tumor progression, epidermal growth factor receptor overexpression, and snail up-regulation. *Clin Cancer Res* 2008; **14**: 4743–50.
22 Fujii K, Luo Y, Sasahira T, Denda A, Ohmori H, Kuniyasu H. Co-treatment with deoxycholic acid and azoxymethane accelerates secretion of HMGB1 in IEC6 intestinal epithelial cells. *Cell Prolif* 2009; **42**: 701–9.
23 Gumbiner BM. Regulation of cadherin-mediated adhesion in morphogenesis. *Nat Rev Mol Cell Biol* 2005; **6**: 622–34.
24 Kimura Y, Furuhata T, Mukaiya M *et al.* Frequent beta-catenin alteration in gallbladder carcinomas. *J Exp Clin Cancer Res* 2003; **22**: 321–8.
25 Neth P, Ries C, Karow M, Egea V, Ilmer M, Jochum M. The Wnt signal transduction pathway in stem cells and cancer cells: influence on cellular invasion. *Stem Cell Rev* 2007; **3**: 18–29.
26 Raimondi C, Gianni W, Cortesi E, Gazzaniga P. Cancer stem cells and epithelial-mesenchymal transition: revisiting minimal residual disease. *Curr Cancer Drug Targets* 2010; **10**: 496–508.
27 Sarkar FH, Li Y, Wang Z, Kong D. Pancreatic cancer stem cells and EMT in drug resistance and metastasis. *Minerva Chir* 2009; **64**: 489–500.
28 Singh A, Settleman J. EMT, cancer stem cells and drug resistance: an emerging axis of evil in the war on cancer. *Oncogene* 2010; **29**: 4741–51.
29 Hirata K, Ajiki T, Okazaki T, Horiuchi H, Fujita T, Kuroda Y. Frequent occurrence of abnormal E-cadherin/beta-catenin protein expression in advanced gallbladder cancers and its association with decreased apoptosis. *Oncology* 2006; **71**: 102–10.
30 Priya TP, Kapoor VK, Krishnani N, Agrawal V, Agrawal S. Role of E-cadherin gene in gall bladder cancer and its precursor lesions. *Virchows Arch* 2010; **456**: 507–14.
31 Koga Y, Kitajima Y, Miyoshi A *et al.* Tumor progression through epigenetic gene silencing of O(6)-methylguanine-DNA methyltransferase in human biliary tract cancers. *Ann Surg Oncol* 2005; **12**: 354–63.
32 Zavadil J, Narasimhan M, Blumenberg M, Schneider RJ. Transforming growth factor-beta and microRNA:mRNA regulatory networks in epithelial plasticity. *Cells Tissues Organs* 2007; **185**: 157–61.
33 Mongroo PS, Rustgi AK. The role of the miR-200 family in epithelial-mesenchymal transition. *Cancer Biol Ther* 2010; **10**: 219–22.
34 Shen Y, Hirsch DS, Sasiela CA, Wu WJ. Cdc42 regulates E-cadherin ubiquitination and degradation through an epidermal growth factor receptor to Src-mediated pathway. *J Biol Chem* 2008; **283**: 5127–37.
35 Georgopoulos NT, Kirkwood LA, Walker DC, Southgate J. Differential regulation of growth-promoting signalling pathways by E-cadherin. *PLoS ONE* 2010; **5**: e13621.
36 Kim S, Schein AJ, Nadel JA. E-cadherin promotes EGFR-mediated cell differentiation and MUC5AC mucin expression in cultured human airway epithelial cells. *Am J Physiol Lung Cell Mol Physiol* 2005; **289**: L1049–60.
37 Qian X, Karpova T, Sheppard AM, McNally J, Lowy DR. E-cadherin-mediated adhesion inhibits ligand-dependent activation of diverse receptor tyrosine kinases. *EMBO J* 2004; **23**: 1739–48.
38 Takahashi K, Suzuki K. Density-dependent inhibition of growth involves prevention of EGF receptor activation by E-cadherin-mediated cell-cell adhesion. *Exp Cell Res* 1996; **226**: 214–22.
39 Xu L, Hausmann M, Dietmaier W *et al.* Expression of growth factor receptors and targeting of EGFR in cholangiocarcinoma cell lines. *BMC Cancer* 2010; **10**: 302.
40 Ariyama H, Qin B, Baba E *et al.* Gefitinib, a selective EGFR tyrosine kinase inhibitor, induces apoptosis through activation of Bax in human gallbladder adenocarcinoma cells. *J Cell Biochem* 2006; **97**: 724–34.

J Gastroenterol
DOI 10.1007/s00535-012-0572-5

ORIGINAL ARTICLE—ALIMENTARY TRACT

Advanced glycation end products (AGE) induce the receptor for AGE in the colonic mucosa of azoxymethane-injected Fischer 344 rats fed with a high-linoleic acid and high-glucose diet

Takasumi Shimomoto · Yi Luo · Hitoshi Ohmori · Yoshitomo Chihara · Kiyomu Fujii · Tomonori Sasahira · Ayumi Denda · Hiroki Kuniyasu

Received: 27 July 2011 / Accepted: 22 February 2012

Abstract
Background Advanced glycation end products (AGE) and the receptor for advanced glycation end products (RAGE) are closely associated with colorectal cancer progression. The association between RAGE and AGE in colon carcinogenesis needs to be clarified.
Methods Levels of RAGE and AGE were examined in azoxymethane (AOM)-injected Fischer 344 rats fed a control diet (Group C), a 15 % linoleic acid (LA) diet (Group L), a control diet with 10 % glucose drink (Group G), and a 15 % LA diet with 10 % glucose drink (Group L + G). Group L + G showed the most pronounced increase of body weight, blood sugar, and serum insulin.
Results The rats in Group L + G showed the most pronounced multiplicity of aberrant crypt foci (ACF) and carcinomas with increased mucosal RAGE and AGE. IEC6 rat intestinal epithelial cells treated with AGE showed increased RAGE expression, which was inhibited by treatment with metformin or losartan. In the AOM-injected rat colon cancer model, the levels of RAGE and AGE, and the multiplicity of ACF and carcinomas, in Group L + G rats were suppressed by treatment with metformin or losartan.
Conclusions These results suggest that AGE–RAGE induced by high-LA and high-glucose diets substantially enhances colon cancer development; thus, suppression of AGE–RAGE could be a potential target for colon cancer chemoprevention.

Keywords Colon carcinogenesis · Linoleic acid · Sugar · AGE

T. Shimomoto · Y. Luo · H. Ohmori · Y. Chihara · K. Fujii · T. Sasahira · A. Denda · H. Kuniyasu (✉)
Department of Molecular Pathology, Nara Medical University, 840 Shijo-cho, Kashihara, Nara 634-8521, Japan
e-mail: cooninh@zb4.so-net.ne.jp

Abbreviations

AGE	Advanced glycation end products
RAGE	Receptor for advanced glycation end products
CRC	Colorectal cancer
LA	Linoleic acid
AOM	Azoxymethane
ROS	Reactive oxygen species
PUFA	Polyunsaturated fatty acid
BSA	Bovine serum albumin
MMP	Matrix metalloproteinase
VEGF	Vascular endothelial growth factor
iNOS	Inducible nitric oxide synthase
ACF	Aberrant crypt foci
HMGB	High mobility group box
NF	Nuclear factor
ERK	Extracellular signal-regulated kinase
JNK	c-Jun N-terminal kinase

Introduction

Advanced end glycation products (AGE) are generated by nonenzymatic reactions under hyperglycemic and oxidative conditions, which are closely linked to high-fat and high-sugar diets [1, 2]. AGE are a major cause of diabetic complications such as retinopathy and nephropathy [3–5]. AGE-associated oxidative stress is one of the causes of genotoxicity [6]. AGE serve as the ligands of receptor for advanced glycation end products (RAGE) [3, 7, 8]. RAGE is a membrane receptor of the immunoglobulin superfamily, which is linked to serine/threonine protein kinases [7, 9]. RAGE enhances the cellular processes associated with cancer progression [10–14]. RAGE-mediated intracellular signaling pathways are associated with cell

Published online: 31 March 2012

proliferation, survival, migration, and invasion; lysis of stroma; angiogenesis; and the generation of oxidative stress [10, 11, 13–17]. Moreover, the above-mentioned processes are induced by the activation of RAGE in epithelial cell transformation. RAGE expression is undetected in the normal colon and stomach mucosa [11, 12]; however, RAGE expression is induced in neoplastic lesions. Induction of RAGE expression is detected particularly during the progression of colon adenoma to colon adenocarcinoma [18].

Western influence on diet has increased the incidence of colorectal cancer (CRC) [19]. Typically, western foods are high in fat and glucose. Accelerated AGE formation due to hyperlipidemia- and hyperglycemia-induced oxidative stresses may predispose an individual to CRC [2, 6]. Hyperglycemia induces reactive oxygen species (ROS) through an increase of glyoxal, glyceraldehyde, methylglyoxal, and pyruvate, which are also associated with AGE formation [20–22]. Metformin and losartan are common drugs used for the treatment of diabetes and hypertension, respectively, and these drugs are reported to possess anti-AGE effects in non-cancerous conditions [23–25]. We intended to clarify their anti-AGE effect on colon cancer development.

Linoleic acid (LA), which is a major component of dietary oil in feed for rodents. In experimental animal models, acts as a synergist for azoxymethane (AOM) in rat colon mucosa. LA in combination with AOM increases the levels of growth-associated proteins in rats [26–28]. Increased dietary intake of LA, which is associated with AGE formation, results in the oxidation of low-density lipoprotein and platelet aggregation and interferes with the incorporation of essential fatty acids in cell membranes, which worsens arterial sclerosis [3, 20, 29]. LA is an omega-6 polyunsaturated fatty acid (PUFA). The dietary ratio of omega-6 PUFAs to omega-3 PUFAs is ideally 1:1; however, the ratio is 50:1 in the western diet [30]. Thus, increased dietary intake of omega-6 PUFAs, such as LA, and sugar is thought to be a vital aspect of the western diet that contributes to the development of colon cancer.

In this study, we attempted to determine the significance of the relation between AGE and RAGE to the development of CRC under conditions of a high-LA and high-glucose diet.

Materials and methods

Animals and diets

Five-week-old male F344 rats (Japan SLC, Shizuoka, Japan) were acclimatized for 1 week and then randomized into experimental and control groups. All animals were housed 4 per wide cage. The holding room was maintained at 23 °C, 50 % humidity, with a 12-h light/12-h dark cycle. A control diet, which contains 2 % LA (CE-2) was purchased from Clea (Tokyo, Japan). The experimental diet was prepared by mixing LA (Wako Pure Chemical Industries, Osaka, Japan) into the CE-2 diet to a 15 % w/w concentration. The ethics of this study was approved by the Committee for Animal Experimentation of Nara Medical University. A 10 % glucose solution for drinking was prepared from 50 % glucose solution for injection (Terumo, Tokyo, Japan) by dilution with distilled water. Metformin (Alexis Biochemicals, San Diego, CA, USA) and losartan (Toronto Research Chemicals, Toronto, Canada) were dissolved in the drinking water. The dosages of metformin and losartan were selected according to the results of a comparison of 3 different dosages. Among metformin dosages of 1.5, 15, and 150 mg/kg body weight/day, the dosage of 15 mg/kg body weight/day produced a decrease of blood sugar but did not cause hypoglycemia or acidotic change. Among losartan dosages of 0.2, 2, and 20 mg/kg body weight/day, the dosage of 2 mg/kg body weight/day produced mild reduction of blood pressure but did not affect behavior or food intake. This experiment was performed as a preliminary experiment to decide the appropriate dosage. Thus, metformin and losartan were used at concentrations of 15 and 2 mg/kg body weight, respectively, in the following in vivo experiments and at 15 and 2 μg/ml, respectively, in cell culture.

Experimental procedure

Two hundred male F344 rats aged 5 weeks old were divided into 4 groups; the control diet (Group C), high-LA diet (15 % LA in control diet, Group L), high-glucose diet (10 % glucose drink and control diet, Group G), and high-LA + high-glucose diet (10 % glucose drink and 15 % LA in control diet, Group L + G). Body weight and food consumption were measured once a week throughout the experimental period. Water intake, urine volume, blood sugar, and serum insulin were examined at week 50 on the day before sacrifice. Rats were sacrificed under ether anesthesia after cardiac blood collection at weeks 0, 4, 8, 16, and 50 after the first AOM injection. In all sacrificed rats, the colon was removed, flushed with normal saline, and opened from the cecum to the anus, to observe neoplastic lesions. In each group, 5 of the 15 colons were fixed flat on a plastic plate in 10 % buffered formalin for histological analysis. ACF were examined according to the method and criteria reported by McLellan et al. [31]. The colon was stained with methylene blue and observed with a stereomicroscope. For the analysis of protein production and mRNA expression, the mucosae were scraped from another 5 colons in each group, frozen under liquid nitrogen, and stored at −80 °C for further analysis.

Sampling of blood

Blood was collected from the rats by cardiac centesis with a 23-G needle. Blood sugar was examined with a Medisafe blood sugar measuring kit (Terumo). The blood was rapidly centrifuged at 500×*g*, for 4 min at 4 °C. The supernatant was used as serum for further examinations.

Enzyme-linked immunosorbent assays (ELISAs) for RAGE, AGE, and insulin

ELISA kits were used for the measurement of the protein concentrations of RAGE (R&D Systems, Minneapolis, MN, USA), AGE (Cusabio Biotech, Wilmington, DE, USA), and insulin (R&D Systems). A small piece (approximately 10 mm^3) of tissue was obtained from each rat colon, frozen with liquid nitrogen, and stored at −80 °C. The tissues were homogenized in lysis buffer (50 mM Tris HCl, pH 7.5, 5 mM ethylenediaminetetraacetic acid [EDTA], 1 mM ethylene glycol tetraacetic acid [EGTA], 2 % nonidet-40, 10 μg/ml leupeptin, 50 μg/ml phenylmethylsulfonyl fluoride), and centrifuged (5000×*g*). The supernatant (10 μg) was used for ELISA. The assay was performed in triplicate and according to the manufacturers' instructions. The experiment was repeated twice.

Immunohistochemistry

Consecutive 4-μm sections were immunohistochemically stained using an immunoperoxidase technique described previously [11]. For antigen retrieval, pepsin (DAKO, Carpinteria, CA, USA) treatment was carried out for 20 min at room temperature. Anti-RAGE antibody (clone C-20; Santa Cruz Biotechnology, Santa Cruz, CA, USA) diluted to 0.5 μg/ml was used as the primary antibody. Secondary antibodies (Medical & Biological Laboratories, Nagoya, Japan) were used at a concentration of 0.2 μg/ml. Specimens were color-developed with diaminobenzidine hydrochloride (DAB; DAKO). Mayer's hematoxylin (Sigma Chemical, St. Louis, MO, USA) was used for counterstaining. Immunostaining of all specimens was performed simultaneously to ensure the same antibody reaction and DAB exposure conditions.

Cell culture

A rat intestinal cell line, IEC6, purchased from Dainihon Pharmaceutical (Tokyo, Japan), was routinely maintained in DMEM (Wako Pure Chemical Industries) containing 10 % fetal bovine serum (FBS) (Whittaker M.A. Bioproducts, Walkersville, MD, USA) under conditions of 5 % CO_2 in air at 37 °C.

Immunoblot analysis

Whole-cell lysates were prepared as described previously [11]. For the extraction of histone, a Histone Purification kit (Active Motif, Tokyo, Japan) was used. Fifty-μg lysate aliquots were subjected to immunoblot analysis using 12.5 % sodium dodecylsulfate (SDS)–polyacrylamide gel followed by electrotransferonto a nitrocellulose filter. The filters were incubated with the primary antibody and then with peroxidase-conjugated anti-goat IgG antibody (Medical and Biological Laboratories, Nagoya, Japan) in the secondary reaction. For internal control of the loaded protein amount, tubulin was detected with a specific antibody (Zymed Laboratories, South San Francisco, CA, USA). The immune complex was visualized using an enhanced chemiluminescence (ECL) western blot detection system (Amersham, Aylesbury, UK). The antibodies used were: anti-RAGE (Santa-Cruz Biotechnology, Santa-Cruz, CA, USA), anti-matrix metalloproteinase (MMP9) (Novocastra Laboratories, Newcastle upon Tyne, UK), anti-vascular endothelial growth factor (VEGF) and anti-inducible nitric oxide synthase (iNOS) (Santa-Cruz Biotechnology), anti-BCL2 (DAKO, Carpinteria, CA, USA), and anti-Hi histone (Active Motif). For semi-quantification, the specific signals on immunoblotted membrane detected by each antibody were computer-captured and quantified with NIH image computer software (National Institutes of Health, Bethesda, MD, USA). The signal intensities were normalized against tubulin expression. The relative expressed was calculated on the basis of the expression in Group C, which was set at 1.

AGE formation

Bovine serum albumin (BSA, 1 mM, fraction V, fatty acid-free, endotoxin-free; Sigma Chemical) was incubated with high-concentration glucose solution (1 M glucose, 1.5 mM phenylmethylsulfonyl fluoride [PMSF], 0.5 μg/ml leupeptin, 2 μg/ml aprotinin, 0.5 mM EDTA, 100 units/ml ampicillin [Sigma Chemical]), and 40 μg/ml streptomycin (Sigma Chemical) at 37 °C for 6 weeks under sterile conditions. After incubation, free glucose and BSA were removed by dialysis against phosphate-buffered saline (PBS) [16, 32]. For examining the cellular formation of AGE, IEC6 cells were treated with a high concentration of glucose (300 mg/dl) and glyoxal (100 μM) [33]. As H1 histone is a well-known glycation target [34], AGE formation of H1 histone was examined by immunoblotting.

Statistical analysis

Statistical significance was examined by the two-tailed, unpaired Mann–Whitney test by using InStat software (Graphpad Software, Los Angeles, CA, USA). Statistical

significance was defined as a two-sided P value of less than 0.05.

Results

Body weight and calorie intake of the rats

The experimental protocol is shown in Fig. 1a. AOM-injected Fischer 344 (F344) rats were divided into the following groups depending on their diet: the control diet group (Group C), the 15 % LA diet group (Group L), the 10 % glucose drink group (Group G), and the 15 % LA with 10 % glucose drink group (Group L + G). The rats in Group L + G showed a 24 % gain in body weight and 67 % higher levels of calorie intake than the rats in Group C at 50 weeks after the AOM injection (Fig. 1b, c).

Water intake, urine, blood sugar, and serum insulin levels in the rats

The volumes of water intake and urine in the rats in Group G and Group L + G were higher than those in the rats in Group C (Fig. 2a, b). The blood sugar levels in the rats in Group G and Group L + G were higher than those in the rats in Group C (Fig. 2c). Serum insulin levels were higher in the rats in Groups G, L, and L + G than those in Group C rats (Fig. 2d). Thus, the rats in Group G and Group L + G showed high water intake, high urine volume, and high blood sugar levels in spite of having high serum insulin levels. In contrast, Group L showed a high serum insulin level but not a high blood sugar level.

Protein levels of RAGE and AGE in nonneoplastic mucosa

In each group, RAGE protein expression in the colonic mucosa was temporally increased; however, RAGE expression in Group L + G was higher than that in the other groups (Fig. 3a–c). RAGE expression increased temporally and reached a peak at week 50 (Fig. 3d). At 50 weeks, the increase in RAGE expression in Group L + G rats was more significant than that in Group C rats. We also examined serum AGE levels (Fig. 3e). At weeks 16 and 50, the AGE levels in Group L + G rats showed a more significant increase than those in Group C rats. Moreover, at week 50, the rats in Groups L and G showed a significantly greater increase in serum AGE level than Group C rats; Group C rats showed no increase in serum AGE levels. In addition, we examined the AGE levels in the colonic mucosa (Fig. 3f). In comparison with Group C rats, the rats in Groups G, L, and L + G showed a

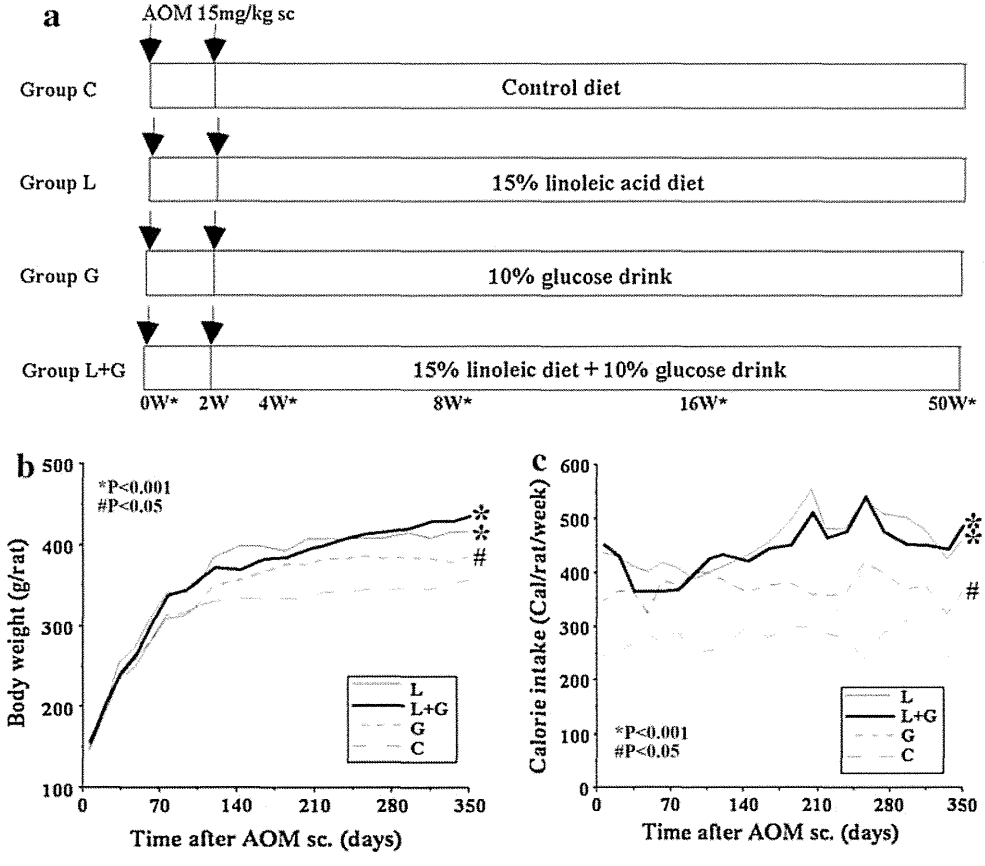

Fig. 1 Azoxymethane (*AOM*)-induced rat colon cancer model. **a** Protocol of the experiment. In each group, 10 rats were prepared at each time point. *Asterisk* shows sacrifice time point. Changes in body weight (**b**) and calorie intake (**c**) over time. The standard error was within 15 % of the indicated mean value. *C* Group C, *G* Group G, *L* Group L, *L + G* Group L + G, *W* week, *sc* subcutaneous

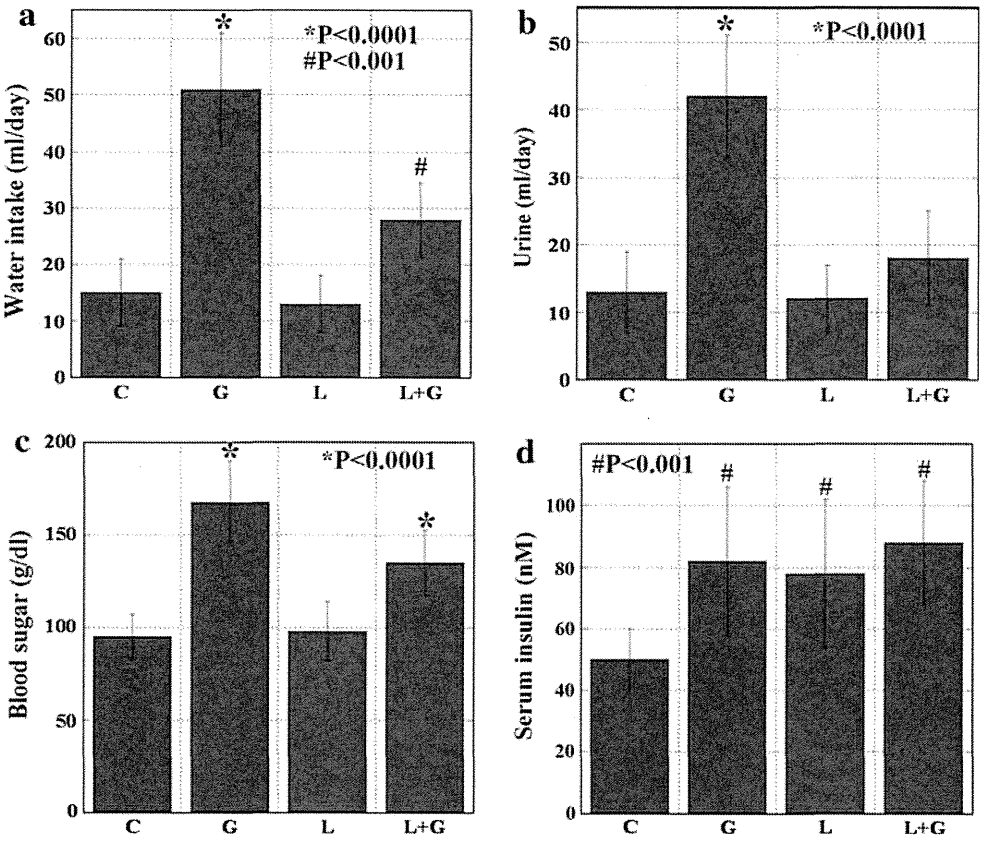

Fig. 2 Biological parameters in azoxymethane-injected rats fed with the high-linoleic acid (LA) and/or high-glucose diets. Water intake (**a**), urine volume (**b**), blood sugar (**c**), and serum insulin (**d**) at week 50. For analysis of water intake and urine volume, mean values were calculated from data obtained over 7 days. Blood samples for blood sugar and serum insulin were obtained at 9 a.m., before the rats were sacrificed. *Error bars* SD. Statistical significance was calculated by comparing the values obtained in Group C with those in the remaining groups

significant increase in AGE levels at weeks 16 and 50. Thus, the levels of RAGE and AGE were increased by high LA and/or high glucose intake.

Development of aberrant crypt foci (ACF) and carcinoma in the colon

All the AOM-injected rats developed ACF and carcinoma in the colon (Table 1). The multiplicity of aberrant crypt foci (ACF) was examined in the rats at week 16. The total number of ACF was higher in the rats in Groups G, L, and L + G than that in the Group C rats. Group L + G in particular showed the highest multiplicity of ACF among the 4 Groups. ACF with more than 9 crypts was also the highest in Group L + G. The multiplicity of carcinomas was examined in the rats at week 50. The number of carcinomas was higher in the rats in Groups G, L, and L + G than that in Group C rats. Moreover, Group L + G showed a higher degree of multiplicity than those in Groups G and L. The formation of ACF and carcinomas was thus increased by high LA and/or high glucose intake.

Expression of RAGE-associated proteins in colon mucosa

The expression profiles of RAGE and RAGE-associated proteins were examined in rat colon mucosa (Fig. 4). We examined the expressions of MMP-9, VEGF, iNOS, and BCL2, all of which are reported to be upregulated by RAGE activation in CRCs [16]. The expressions of RAGE and MMP9 were both upregulated in Groups G, L, and L + G in comparison with Group C. The expressions of iNOS and BCL2 were both upregulated in Groups L and L + G in comparison with Group C. VEGF expression in Group L + G was upregulated in comparison with that observed in Group C. Group L + G showed the highest levels of these proteins among the 4 groups. The levels of RAGE and its associated proteins were upregulated by high LA and/or high glucose intake.

Upregulation of RAGE by AGE

IEC6 rat intestinal cells were treated with glycated-BSA (AGE-BSA) (Fig. 5a). RAGE production in AGE-BSA-treated IEC6 cells was upregulated in a dose-dependent manner. Cellular AGE formation and RAGE protein levels were examined in IEC6 cells, using co-treatment with high glucose (300 mg/dl) and glyoxal (100 μM) for 0, 2, and 6 weeks. H1 histone increased the molecular weight by modification of AGE [16]. At weeks 2 and 6, RAGE expression was upregulated in IEC6 cells. In contrast, in IEC6 cells treated concurrently with high glucose plus glyoxal and metformin or losartan, AGE formation and RAGE levels were decreased in comparison with those in

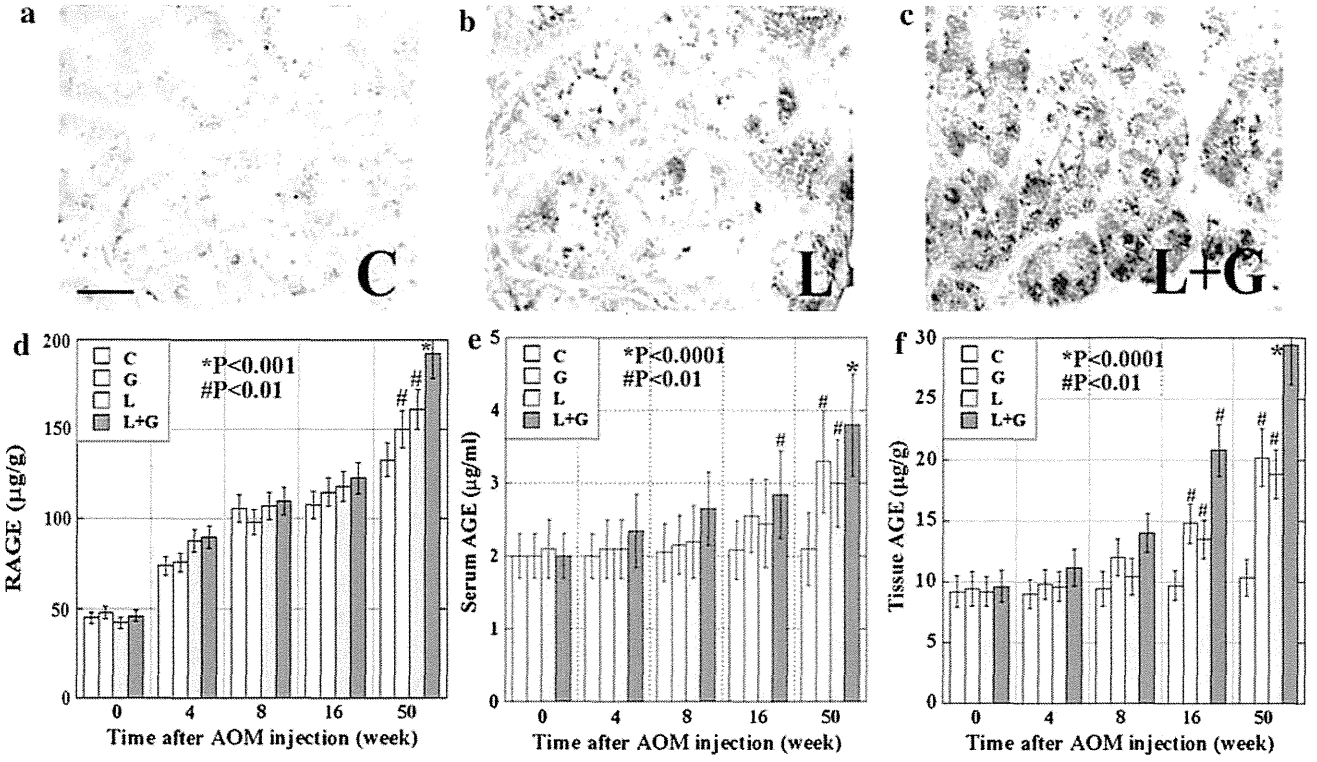

Fig. 3 Expressions of receptor for advance glycation end products (RAGE) and AGE in the colonic mucosa of azoxymethane-injected rats. **a–c** RAGE protein expression was examined by immunohistochemistry in the rat mucosa at week 16. Time course of the expression levels of mucosal RAGE (**d**), serum AGE (**e**), and mucosal AGE (**f**). *C* Group C, *G* Group G, *L* Group L, *L* + *G* Group L + G. *Bar* in **a** 50 μm. *Error bars* SD. Statistical significance was calculated by comparing the values obtained in Group C with those obtained in the remaining groups

Table 1 Numbers of aberrant crypt foci and carcinoma in rats

	Group C	Group G	Group L	Group L + G
Aberrant crypt foci at week 16				
Number of rats	10	10	10	10
Crypt number				
Total	146 ± 16	180 ± 20[a,c]	208 ± 28[b]	256 ± 30[b]
1–3	124 ± 14	144 ± 16[a,c]	164 ± 20[b,d]	184 ± 22[b]
4–8	18 ± 3	28 ± 4[b,c]	32 ± 4[b,c]	56 ± 8[b]
9–	4 ± 0.8	8 ± 1.6[b,c]	12 ± 2[b,d]	16 ± 4[b]
Carcinoma at week 50				
Number of rats	10	10	9	10
	4 ± 1.6	6.3 ± 1.8[a,c]	9.2 ± 2.1[b,d]	11.6 ± 2.7[b]

[a,b] Significant differences between Group C and Group G, Group C and Group L, and Group C and Group L + G; [a]$P < 0.01$, [b]$P < 0.001$

[c,d] Significant differences between Group L + G and Group G, and Group L + G and Group L; [c]$P < 0.01$, [d]$P < 0.05$

untreated cells (denoted as "None" in Fig. 5c). AGE formation and RAGE production were examined by ELISA at week 6. Cells treated with high glucose plus glyoxal showed increases of AGE and RAGE. In contrast, cells treated concurrently with high glucose plus glyoxal and metformin or losartan showed lower levels of AGE and RAGE than those in untreated cells ("None" in Fig. 5c). These results suggest that RAGE was upregulated by AGE, and this upregulation was inhibited by metformin or losartan.

Effect of RAGE knockdown on the number of ACF in AOM-treated rats

To confirm the pivotal role of RAGE in colon carcinogenesis, we examined the effect of RAGE knockdown on colon cancer development (Fig. 6). We administered RAGE small interfering RNA (siRNA) and counted the multiplicity of ACF at week 16 in AOM-treated F344 rats fed with the high-LA diet and glucose drink (Fig. 6a). A total of 22 administrations of RAGE siRNA (Group KD)

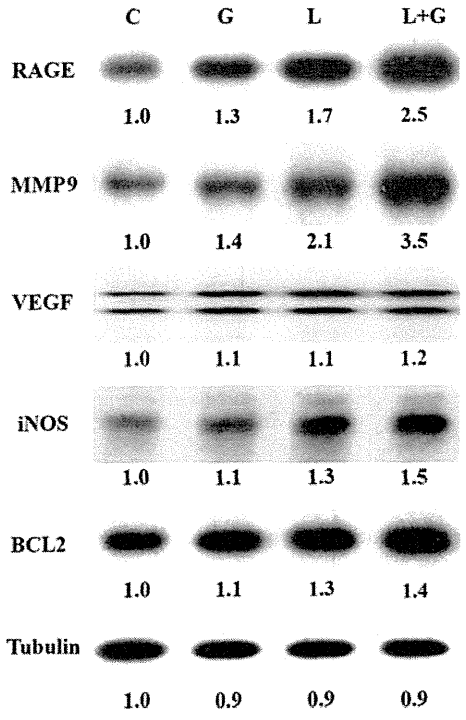

Fig. 4 Expression of RAGE and RAGE-associated proteins in colon mucosa. Expression of RAGE proteins and associated genes in colon mucosa was examined at 16 weeks by immunoblotting. *Numbers* protein levels normalized against tubulin expression and expressed as a relative value on the basis of the expression in Group C, which was set at 1.0. *MMP* matrix metalloproteinase, *VEGF* vascular endothelial growth factor, *iNOS* inducible nitric oxide synthase

reduced RAGE production to 9 % of that in Group L + G at week 16 (Fig. 6b). The total number of ACF and the number of ACF with 4 or more crypts were decreased by RAGE knockdown (Fig. 6c). Thus, we concluded that RAGE was involved in colon carcinogenesis.

Effect of metformin and losartan on formation of ACF and carcinomas in AOM-treated rats

We examined the effects of metformin and losartan on the formation of ACF and carcinoma in the colons of rats fed with high LA and high glucose, and found that the colonic mucosa in these rats showed high levels of AGE and RAGE (Fig. 7). In rats treated with metformin the multiplicity of ACF was reduced in comparison with that in Group L + G rats at week 16 (Fig. 7b). In contrast, rats treated with losartan did not show a significant change of ACF multiplicity in comparison with that in the rats in Group L + G. In contrast to ACF formation at week 16 and the number of carcinomas at week 50, ACF formation and the number of carcinomas were reduced in rats treated with metformin or losartan in comparison to these parameters in Group L + G (Fig. 7c). Serum AGE was reduced in metformin-treated rats from week 8 in comparison with Group L + G rats; in contrast, at week 50, serum AGE was reduced in the losartan-treated rats only (Fig. 7d). The levels of mucosal RAGE in the metformin-treated rats were decreased in comparison with the rats in Group L + G from week 16; in contrast, a decrease was observed in losartan-treated rats at week 50 (Fig. 7e). Thus, in rats treated with metformin and losartan the multiplicity of ACF and/or carcinomas was reduced. This reduction was associated with decreased AGE and RAGE in rats fed with the high-LA and high-glucose diets.

Discussion

In the present study, we showed that AGE and RAGE were upregulated in the colonic mucosa of AOM-injected F344 rats, especially in rats fed with high-linoleic acid (LA) and high-glucose diets, and this upregulation was associated with increased ACF and carcinomas in the rat colon. We examined the effect of dietary LA and glucose on AOM-induced colon carcinogenesis to simulate the western diet. The dietary intake of abundant fat and sugar is a common feature of the western diet, and it is not possible to separate the effects of these two factors in the diet [35]. The ratio of omega-6 PUFA to omega-3 PUFA was reported to be up to more than 50:1 in the western diet [30]. In the present experiment, the ratio in the control diet was 5:1, whereas the ratio in the high-LA diet was 40:1, which approximated that in the western diet. Rats in Groups G and L + G, fed with high glucose, showed significant weight gain and hyperglycemia with hyperinsulinemia; all these findings suggest that the rats suffered from a condition resembling glucose intolerance and insulin resistance, both of which factors are relevant to the western diet. In our model, therefore, the design of Group L + G may represent the typical situation of a western diet. The two factors of glucose intolerance and insulin resistance are also associated with an increase of CRCs [36]. We showed that the multiplicity of ACF and carcinomas was significantly increased in the rats fed with high glucose and/or high LA, especially in rats fed with both. The above two factors thus act relevantly in the development of colon cancer.

We showed that AGE formation induced RAGE expression. In endothelial cells, hyperglycemia induces RAGE and ligands such as high mobility group box (HMGB)-1 and S100 by the generation of ROS through nuclear factor (NF) κB [21]. Diabetic hyperglycemia nonenzymatically forms AGE, which induces RAGE expression [37]. The RAGE gene promoter contains binding sites for NFκB and specificity protein 1 (SP-1) [38, 39]. NFκB is activated by hyperglycemia, oxidative stress, AGE, and RAGE activation itself, which conditions induce RAGE expression in a complicated manner, such that they

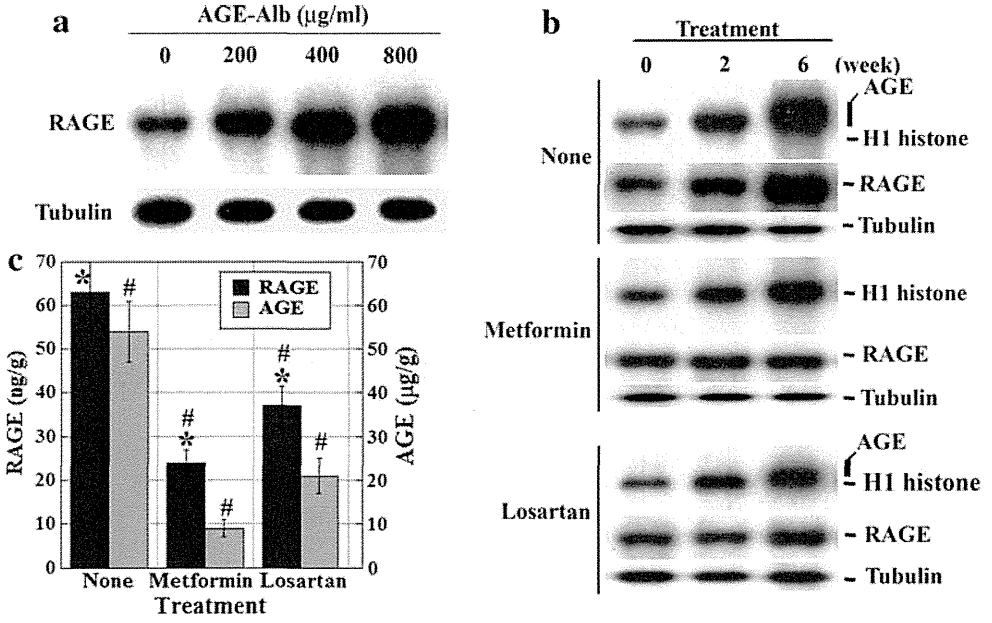

Fig. 5 RAGE induction by AGE in IEC6 cells. **a** RAGE expression in IEC6 cells treated with AGE-bovine serum albumin (BSA) for 48 h. **b**, **c** Cellular AGE formation and RAGE protein levels were examined in IEC6 cells treated with high glucose (300 mg/dl) and glyoxal (100 μM). **b** Cellular AGE formation of H1 histone and RAGE production were examined by immunoblotting in IEC6 cells with and without metformin or losartan treatment at weeks 0, 2, and 6. Tubulin served as a loading control. **c** Concentration of AGE and RAGE in IEC6 cells at week 6. *Error bar* SD. *Asterisk* shows significant difference in RAGE concentration compared with that in cells cultured in standard medium ($P < 0.05$). *Hash symbol* shows statistically significant difference in AGE concentration compared with that in cells treated with high glucose and glyoxal ($P < 0.01$)

Fig. 6 Effect of RAGE knockdown on the number of aberrant crypt foci in azoxymethane-injected rats. **a** Experimental protocol. In each group, 10 rats were examined. **b** RAGE protein levels were examined by immunoblotting. Tubulin was examined as a loading control. **c** Multiplicity of aberrant crypt foci (*ACF*) in the colon at week 16. *Bar* SD. *siRNA* short interfering RNA

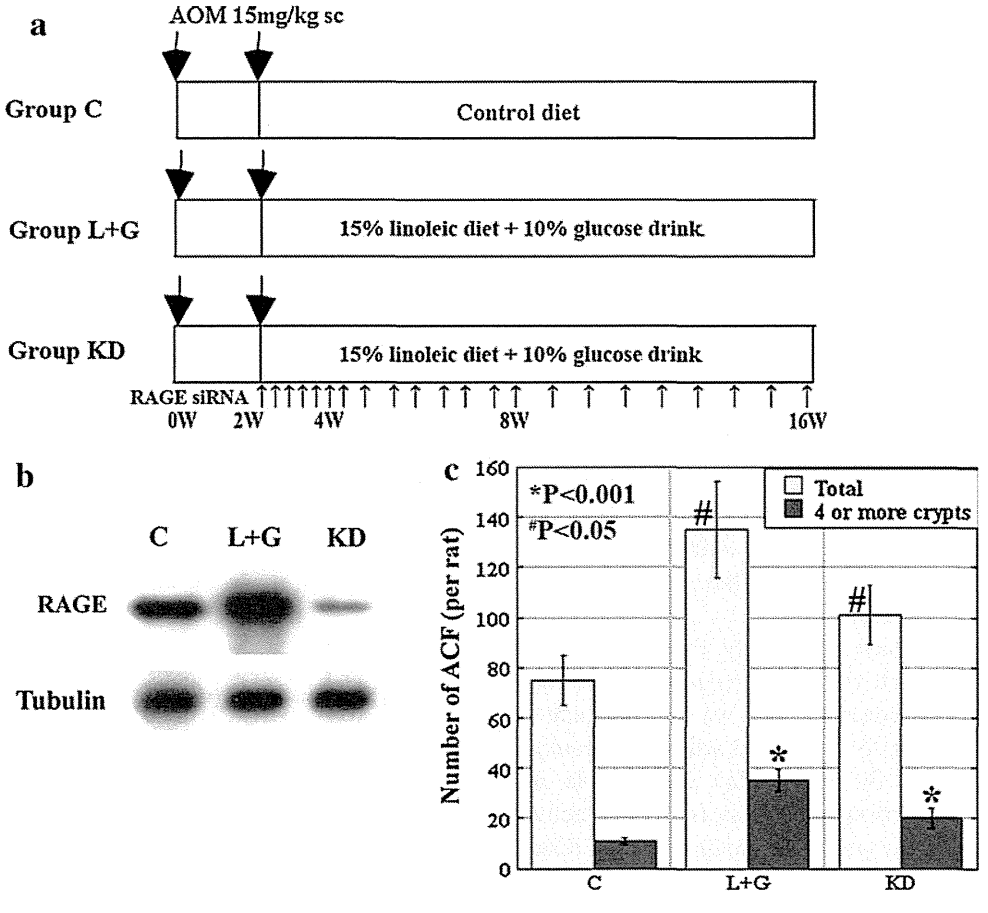

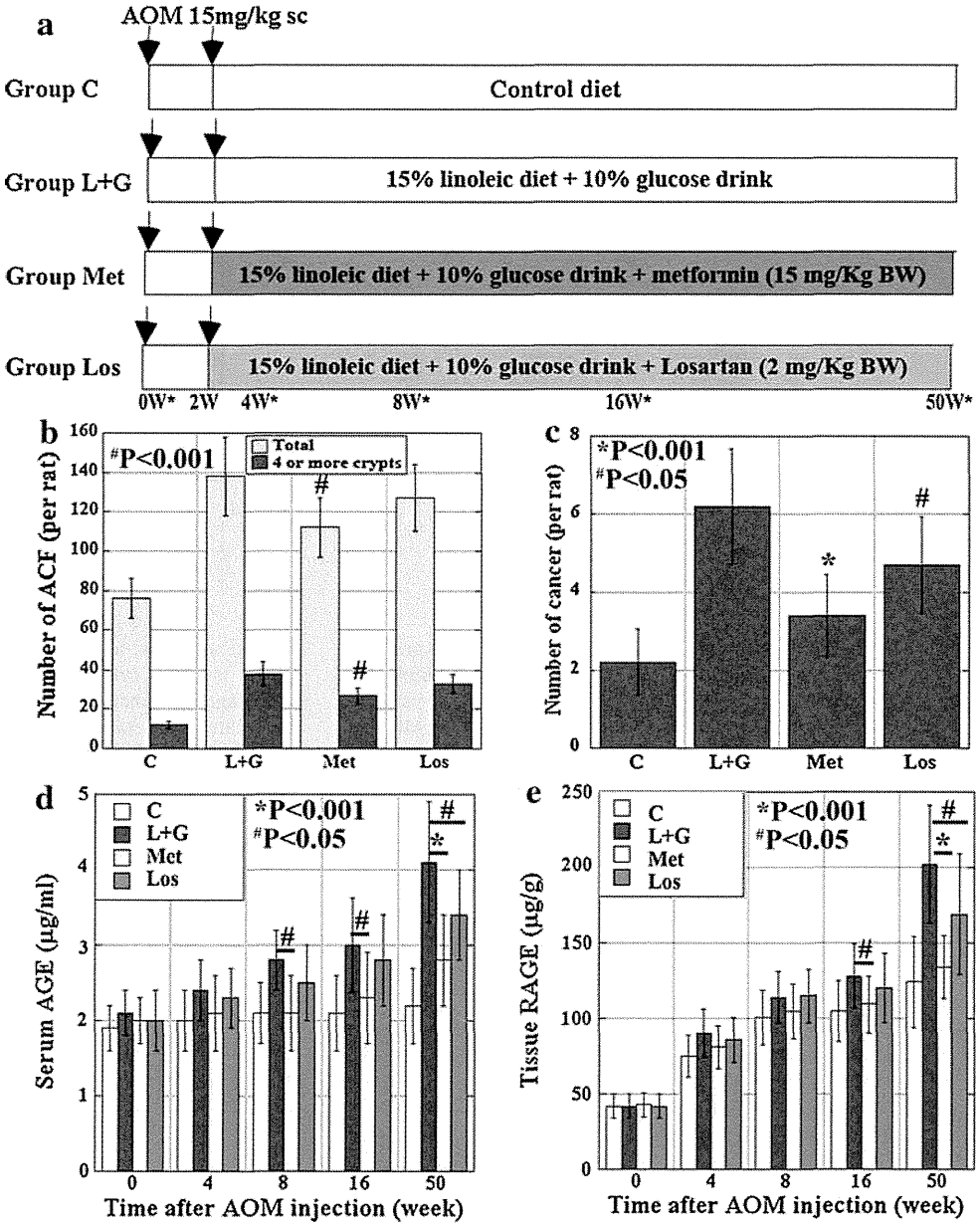

Fig. 7 Effects of metformin and losartan on levels of AGE and RAGE in azoxymethane-injected rats. **a** Experimental protocol. In each group, 10 rats were prepared at each time point. *Asterisk* shows sacrifice time point. **b** Multiplicity of aberrant crypt foci (ACF) in the colon at week 16. **c** Multiplicity of adenocarcinomas in the colon at week 50. Time course of serum AGE (**d**) and mucosal RAGE (**e**) in azoxymethane (AOM)-injected rats. *BW* body weight, *C* Group C (control diet-fed), *L + G* Group L + G [fed with high linoleic acid (LA) and high glucose], *Met* Group M (L + G with metformin), *Los* Group L (L + G with losartan treatment). *Error bars* SD. Statistical significance was calculated by comparing the values obtained in Group L + G with those obtained in other groups

generate a positive feedback loop [40]. RAGE activation activates NFκB and iNOS to generate ROS and NO, which accelerate the formation of AGE [1, 2, 6, 41]. Thus a positive feedback loop for AGE formation is also provided. Moreover, continuous oxidative stresses generated by the RAGE–AGE system have the potential to cause DNA damage [6].

We have previously reported that RAGE is closely associated with CRC progression and metastasis [12, 16]. In the present study, we revealed that RAGE was also significantly associated with colon carcinogenesis. Therefore RAGE might play a vital role in CRC from its development to metastasis. RAGE activates intracellular signaling pathways involving Rac1/Cdc42, extracellular signal-regulated kinase (ERK) 1/2, c-Jun N-terminal kinase (JNK), Bcl-2, and NFκB [3, 8, 15]. We confirmed the upregulation of RAGE-associated genes, including MMP9, VEGF, iNOS, and BCL2 in the carcinomas in Group L + G rats. These RAGE-associated multiple pathways bring about the accelerated growth and migration of cancer cells while suppressing apoptosis, all of which contribute to the progression and metastasis of CRC cells [10, 12, 16].

Oxidative stresses induce RAGE ligands such as HMGB1 and S100 [21]. We verified the high concentration of HMGB1 in the colonic mucosa of Group L + G rats [42]. RAGE is concurrently activated by AGE and HMGB1, which exert different effects on the expression of RAGE-associated genes [16]. The phosphorylation of ERK1/2, Rac1, and AKT, and the production of MMP9 are increased more by HMGB1 than by AGE, whereas the

production of iNOS and NFκB is increased more by AGE than by HMGB1. The high-LA and high-glucose diet we used in the present study would therefore have induced a synergistic effect of AGE and HMGB1.

Advanced glycation end products (AGE) are formed by hyperglycemic and/or oxidative conditions in both noncellular and cellular systems. Metformin and losartan reduced AGE formation in noncellular and cellular systems and decreased RAGE induction by AGE in IEC6 cells. Metformin is a commonly used antidiabetic drug used to increase insulin sensitivity. Abrogation of AGE by metformin is reported in osteoblasts and endothelial cells [23, 24]. Losartan, a blocker of angiotensin II type 1 receptor, inhibited nephrectomy-induced AGE formation [25]. These agents reduced both ROS formation by AGE and AGE-induced inactivation of angiotensin II [24, 43, 44]. We found that metformin caused inhibition of AGE formation in noncellular and cellular systems. In contrast, losartan showed mild inhibition of AGE formation in a noncellular system, suggesting that losartan possesses a weak antioxidative effect independent of its anti-angiotensin activity. In a cellular system, losartan showed more pronounced inhibition of AGE formation, which is thought to be Losartan's anti-inflammatory effect via angiotensin antagonism with suppression of NFκB [44]. We previously reported that a cyclooxygenase (COX)-2 inhibitor reduced RAGE expression in 4-nitroquinoline 1-oxide-induced rat tongue cancer [45].

The formation of AGE is accelerated by oxidative stress, and oxidative stress is generated by AGE-activated RAGE, in a self-perpetuating cycle [6]. AGE stimulates ROS production via the activation of nicotinamide adenine dinucleotide phosphate (NADPH) oxidase [46]. In the present study, we found that AGE concentration was increased in the colonic mucosa. AGE formed in tissues or cells may induce continuous ROS production and persistent cellular damage. We found that treatment with metformin and losartan inhibited AGE and reduced cancer multiplicity in the L + G rats in comparison to the control rats (Group C). The blockade of AGE formation and inhibition of AGE effects will be major targets of future therapeutic methods for a number of diseases associated with the western diet [47, 48].

Conflict of interest We declare that there is no financial support and no relationships which may pose a conflict of interest in the contents of the submitted manuscript. All authors have approved the comments.

References

1. Lalla E, Lamster IB, Schmidt AM. Enhanced interaction of advanced glycation end products with their cellular receptor RAGE: implications for the pathogenesis of accelerated periodontal disease in diabetes. Ann Periodontol. 1998;3:13–9.
2. Hori O, Yan SD, Ogawa S, Kuwabara K, Matsumoto M, Stern D, et al. The receptor for advanced glycation end-products has a central role in mediating the effects of advanced glycation end-products on the development of vascular disease in diabetes mellitus. Nephrol Dial Transplant. 1996;11:13–6.
3. Schmidt AM, Hofmann M, Taguchi A, Yan SD, Stern DM. RAGE: a multiligand receptor contributing to the cellular response in diabetic vasculopathy and inflammation. Semin Thromb Hemost. 2000;26:485–93.
4. Yamagishi S, Takeuchi M, Inagaki Y, Nakamura K, Imaizumi T. Role of advanced glycation end products (AGEs) and their receptor (RAGE) in the pathogenesis of diabetic microangiopathy. Int J Clin Pharmacol Res. 2003;23:129–34.
5. Yamamoto Y, Yamagishi S, Yonekura H, Doi T, Tsuji H, Kato I, et al. Roles of the AGE–RAGE system in vascular injury in diabetes. Ann N Y Acad Sci. 2000;902:163–70.
6. Abe R, Yamagishi S. AGE–RAGE system and carcinogenesis. Curr Pharm Des. 2008;14:940–5.
7. Schmidt AM, Yan SD, Wautier JL, Stern D. Activation of receptor for advanced glycation end products: a mechanism for chronic vascular dysfunction in diabetic vasculopathy and atherosclerosis. Circ Res. 1999;84:489–97.
8. Huttunen HJ, Fages C, Rauvala H. Receptor for advanced glycation end products (RAGE)-mediated neurite outgrowth and activation of NF-κB require the cytoplasmic domain of the receptor but different downstream signaling pathways. J Biol Chem. 1999;274:19919–24.
9. Huttunen HJ, Fages C, Kuja-Panula J, Ridley AJ, Rauvala H. Receptor for advanced glycation end products-binding COOH-terminal motif of amphoterin inhibits invasive migration and metastasis. Cancer Res. 2002;62:4805–11.
10. Taguchi A, Blood DC, del Toro G, Canet A, Lee DC, Qu W, et al. Blockade of RAGE–amphoterin signalling suppresses tumour growth and metastases. Nature. 2000;405:354–60.
11. Kuniyasu H, Oue N, Wakikawa A, Shigeishi H, Matsutani N, Kuraoka K, et al. Expression of receptors for advanced glycation end-products (RAGE) is closely associated with the invasive and metastatic activity of gastric cancer. J Pathol. 2002;196:163–70.
12. Kuniyasu H, Chihara Y, Takahashi T. Co-expression of receptor for advanced glycation end products and the ligand amphoterin associates closely with metastasis of colorectal cancer. Oncol Rep. 2003;10:445–8.
13. Kuniyasu H, Chihara Y, Kondo H, Ohmori H, Ukai R. Amphoterin induction in prostatic stromal cells by androgen deprivation is associated with metastatic prostate cancer. Oncol Rep. 2003;10:1863–8.
14. Bhawal UK, Ozaki Y, Nishimura M, Sugiyama M, Sasahira T, Nomura Y, et al. Association of expression of receptor for advanced glycation end products and invasive activity of oral squamous cell carcinoma. Oncology. 2005;69:246–55.
15. Huttunen HJ, Kuja-Panula J, Sorci G, Agneletti AL, Donato R, Rauvala H. Coregulation of neurite outgrowth and cell survival by amphoterin and S100 proteins through receptor for advanced glycation end products (RAGE) activation. J Biol Chem. 2000; 275:40096–105.
16. Kuniyasu H, Chihara Y, Kondo H. Differential effects between amphoterin and advanced glycation end products on colon cancer cells. Int J Cancer. 2003;104:722–7.
17. Sasahira T, Kirita T, Bhawal UK, Ikeda M, Nagasawa A, Yamamoto K, et al. The expression of receptor for advanced glycation end products is associated with angiogenesis in human oral squamous cell carcinoma. Virchows Arch. 2007;450:287–95.
18. Sasahira T, Akama Y, Fujii K, Kuniyasu H. Expression of receptor for advanced glycation end products and HMGB1/amphoterin in colorectal adenomas. Virchows Arch. 2005;446: 411–5.